https://doi.org/10.5194/egusphere-2023-2827
Preprint. Discussion started: 4 January 2024

Satellite Observations Reveal Northern California Wildfire Aerosols Reduce Cloud Cover in California and Nevada Through Semi-Direct Effects

James L. Gomez[1], Robert J. Allen[1], and King-Fai Li[1]
[1]University of California, Riverside
Correspondence: James Gomez (jgome222@ucr.edu)

Abstract. Wildfires in the southwestern United States, particularly in northern California (nCA), have grown in size and severity in the past decade. As they have grown larger, they have been associated with large emissions of absorbing aerosols in to the troposphere. Utilizing satellite observations from MODIS, CERES, AIRS, and CALIPSO, the meteorological effects of aerosols associated with fires during the wildfire season (June-October) were discerned over the nCA-NV (northern California and Nevada) region in the 2003-2022 time frame. As higher temperatures and low relative humidity RH dominate during high surface pressure p_s atmospheric conditions, the effects of the aerosols on high (90th percentile) fire days compared to low fire (10th percentile) days were stratified based on whether p_s was anomalously high or anomalously low (10th percentile). An increase in tropospheric temperatures was found to be concurrent with more absorbing aerosol aloft, which is associated with significant reductions in tropospheric RH during both 90th and 10th percentile p_s conditions. Furthermore, high fire days under low p_s conditions are associated with reduced cloud fraction CF, which is consistent with the traditionally-defined aerosol-cloud semi-direct effect. The reduced CF, in turn, is associated with reduced $TOA\ SW$ radiative flux, a warmer surface, and less precipitation. These changes could create a positive feedback that could intensify fire weather, and therefore extend fire lifetime and impacts.

1 Introduction

As a result of climate change, land use change, and forest management, frequency and severity of wildfires in the southwestern Unites States (US) have trended upwards over the last decade (Li & Banerjee, 2021; Brown et al., 2023), and are projected to increase in coming years due to intensified drought and heatwaves (Goss et al., 2020; Palinkas, 2020; Ager et al., 2021; United Nations Environment Programme, 2022). In both higher and lower CO_2 mitigation scenarios, large wildfire events are projected to become more commonplace by the end of the 21st century worldwide, as well in the southwestern US (United Nations Environment Programme, 2022). Large wildfire events in the late 2010's and early 2020's, known as "mega-fires", were associated with more intense "fire weather": high temperatures T, low relative humidity RH, and high surface wind speeds U_s (Varga et al., 2022; Keeley & Syphard, 2019). These fire weather conditions may be potentially intensified, or alleviated, by the fires themselves. As fires combust vegetation, they emit biomass burning (BB) aerosols such as black carbon (BC), organic aerosols (OA), and brown carbon. Higher burn severity wildfires, such as the 2020 wildfires in California (CA),

https://doi.org/10.5194/egusphere-2023-2827
Preprint. Discussion started: 4 January 2024

have been observed to inject smoke plumes higher into the troposphere than in previous years (Wilmot et al., 2022). These smoke plumes consist of both shortwave (SW) absorbing aerosols such BC and reflective aerosols such as OA, as well as brown carbon, which is both absorbing and reflective. Additionally, they may contain other aerosols aside from BB aerosols, such as dust(Wagner et al., 2021, 2018), which also has SW absorbing properties (Highwood & Ryder, 2014). The absorbing properties of wildfire smoke over the western US, measured using absorbing aerosol optical depth (AAOD), is uncertain. However, a recent study of CA fires indicates that wildfires increase AAOD relative to the annual mean by tenfold (Cho et al., 2022). An injection of absorbing aerosols into the troposphere may cause a local warming affect, altering the hydrological and radiative balance of the atmosphere. Smoke plumes that reach the upper troposphere (pressures$<$500 hPa) may deposit absorbing aerosols that could burn off high clouds, and promote more stable low clouds (Stjern et al., 2017; Smith et al., 2018; Allen et al., 2019), leading to SW and longwave (LW) cooling, an effect also observed to occur with methane SW absorption (Allen et al., 2023). Alternatively, if the absorbing aerosols are concurrent with low clouds, the relative humidity of the liquid cloud layer would be decreased, burning off low clouds and leading to increased SW forcing (Koch & Del Genio, 2010; Allen & Sherwood, 2010). Additionally, the higher injection of absorbing aerosol may alter cloud microphysics, which also has the potential to change the radiative balance of the surface and atmosphere. An influx of aerosols into the troposphere may create an abundance of cloud condensation nuclei (CCN) for droplets to condense onto, decreasing effective radius R_{eff} of the clouds, an effect already observed with smoke (OA/BC) particles in the northwestern US (Twohy et al., 2021). A decrease in R_{eff} would increase the albedo of the clouds, assuming constant water path, which would then increase outgoing SW radiation.

As the western US, and other parts of the world, enter this new regime of mega-fires, there comes a need for improved understanding of the effects of aerosols primarily and secondarily emitted by wildfires. Models participating in the Coupled Model Intercomparison Project version 6 (CMIP6) (Eyring et al., 2016) do not have parametrizations of BB aerosol emissions that respond to CO_2 emissions in most of their experiments, including the DECK (Diagnosis, Evaluation, and Characterization of Klima) experiments (Gomez et al., 2023). Instead, modellers rely on prescription of BB aerosols in these experiments. Recent modelling experiments have found significant effects of wildfires on regional and global climate scales. Previously, using prescribed aerosol simulations in the Community Earth System Model version 2 (CESM2), it was hypothesized that the large 2019 wildfires in Australia could have intensified that year's La Niña through aerosols directly cooling the ocean surface (Fasullo et al., 2021). Another CMIP6 study observed a similar effect on La Niña as a result of a teleconnection caused by an influx of absorbing aerosols into the atmosphere from South African wildfires (Amiri-Farahani et al., 2020). While studies such as these demonstrate that it is possible to model past effects of fires on local and global climate, without proper parameterization of BB aerosol emission, as well as parametrization of secondary dust aerosol emission from wildfire-cleared vegetation, the radiative forcing of future fires' primary and secondary aerosols will remain a source of uncertainty. Therefore, to further motivate the need to incorporate interactive aerosol emissions from wildfires in climate models, as well as to further understand the effects of wildfires on the climate of one of the most populated areas in the US, this paper aims to quantify the radiative as well as microphysical effects that these aerosols have in the region under different atmospheric conditions utilizing satellite data.

https://doi.org/10.5194/egusphere-2023-2827
Preprint. Discussion started: 4 January 2024

2 Satellite and Other Observational Data

The objective of this analysis is to determine how cloud properties differ as a result of primary and secondarily emitted wildfire aerosols over the southwestern US using satellite observations from the Aqua and Cloud-Aerosol Lidar and Infrared Pathfinder Satellite Observation (CALIPSO) (Winker, 2019; Tackett et al., 2018) satellites, as well as fire dry matter emission data DM from the Global Fire Emissions Database (GFED) (van der Werf et al., 2017; Randerson et al., 2017). All data sets are level 3 globally gridded data sets, with the exception of GFED which is considered a level 4 globally gridded dataset.

2.1 Global Fire Emissions Database (GFED)

GFED emissions are calculated in the Carnegie–Ames–Stanford Approach (CASA) model, which requires MODIS burned area data, meteorological data from the ERA-Interim reanalysis dataset, photsynthetically active radiation data based on Advanced Very High Resolution Radiometer satellite instrument retrievals, and vegetation continuous fields data from the MODIS MOD44B dataset (van der Werf et al., 2017). The model is run using burned area data from combined MODIS-Aqua and MODIS-Terra level 3 data (MCD64A1). Use of a burned area based dataset is preferable to a fire power dataset for this paper, as cloud cover may obstruct fire power data retrievals, leading to an underestimation of fire size/severity on a given day. This underestimation is demonstrated in **Figure S2**, which indicates that Aqua fire power retrievals underestimate fire severity compared to DM with 98$\%$ of days reporting a lower normalized fire power than normalized DM. Therefore, for fire power to be a more useful metric, a daily combined Aqua/Terra dataset would have to be used, which is not available for the time frame of interest. GFED fire emissions are also preferred over fire power data and raw burned area data as calculation of fire emissions takes vegetation type and net primary production into account. Raw burned area and fire power datasets yield information about fire size and intensity, but as aerosol emission also depends on the type of vegetation being burned, use of either dataset over a fire emissions dataset may under-estimate or over-estimate biomass burning aerosol impacts on clouds. However, use of GFED data has drawbacks. While use of burned area data reduces the chance of an underestimation of fire impacts, a temporal uncertainty is introduced. This temporal uncertainty is ± 1 day for clear sky conditions, ± 5 days under consistent 75$\%$ cloud cover, and up to ± 20 days over persistently very cloudy (85$\%$ or higher) intervals (Giglio et al., 2013). However, this temporal uncertainty is likely of little significance for this paper, as cloud cover over the western US during the wildfire season is rarely persistently high (aside from "June gloom" in coastal regions), and the lifetime of biomass burning aerosols (roughly 4-12 days) is generally greater than or equal to the temporal uncertainty of clear sky or persistently cloudy burned area data (Cape et al., 2012). Additionally, as the output from GFED is from an older model, which may introduce additional uncertainty. As a result, caution must be taken when analyzing the results. To ensure results are accurate, the GFED DM stratification method was verified by analyzing AOD anomalies during large fire events (Section 3.3, Section 4.2), and by performing cross correlations between AOD and DM (Supplement section 1). GFED emissions and burned area data are available from 1997-2016. Data for 2017-2022 is also available, but the data is in "beta" and therefore is more limited. Both the complete and the beta data contain total carbon emissions, as well as dry matter emission. GFED also estimates the contribution of 6 different types of vegetation biomes (boreal forest, temperate forest, grassland, agriculture, and peat) to the carbon and dry matter emissions.

https://doi.org/10.5194/egusphere-2023-2827
Preprint. Discussion started: 4 January 2024

However the beta dataset only estimates these contributions for DM. Therefore, DM is used as a proxy for the severity of a given fire's emissions, as it is the only variable that both the complete and beta data contain and speciate. All other datasets utilized in this project have a 1^o resolution, however GFED emission data is of a 0.25^o resolution. Therefore, this data was regridded to a 1^o grid.

2.2 Aqua

MODIS-Aqua: Cloud and aerosol optical depth (AOD) data were derived from Moderate Resolution Imaging Spectroradiometer (MODIS) level 3 data. Specifically, the MODIS collection 6.1 1^o level 3 product (MYD08_D3) (Platnick et al., 2003; Salomonson et al., 2002; MODIS Atmosphere Science Team, 2017) is utilized, which yields daily retrieval products from the Aqua satellite. For MODIS cloud retrievals during periods of large AOD, especially when the aerosols are concurrent with clouds, it is possible for MODIS to misidentify aerosols as clouds (Herbert & Stier, 2023). This may cause errors in cloud property retrievals, as well as an overestimation of cloud fraction CF. This may lead to overestimation of CF during anomalously large fire events. While the MODIS Dark-Target and Deep Blue AOD algorithms are extensively quality controlled and evaluated (Levy et al., 2013; Platnick et al., 2017; Wei et al., 2019), there is still room for errors in AOD and cloud retrieval. Additionally, as it is not possible to distinguish wildfire AOD from other AOD, whenever possible fire emissions from GFED are used to discern the impacts of fires on cloud properties.

AIRS: Data concerning T and RH profiles, as well as surface temperature T_s and surface relative humidity RH_s, were derived from Atmospheric Infrared Sounder (AIRS) level 3 daily data (AIRS3STD) (AIRS Science Team & Texeira, 2013). AIRS collects data on an ascending (morning) a descending (afternoon/evening) overpass. For this paper, the descending data was used as it is more temporally consistent with the MODIS derived cloud properties, and the data was associated with lower standard errors than the ascending data for the region of interest.

CERES: Top of atmosphere radiative flux data was derived from Clouds and the Earth's Radiant Energy System (CERES) level 3 time-interpolated daily data Aqua edition (SSF1deg-Day)(Wielicki et al., 1998; Doelling, 2016). The SSF1deg dataset also has auxillariary variables that are computed using the Goddard Earth Observing System (GEOS) model. From this subset of data, surface pressure p_s and U_s variables are derived. AIRS also has a p_s variable which is calculated from a model. The model that AIRS utilizes for p_s calculation is the National Centers for Environmental Prediction Global Forecast System. Comparison of both variables yields very similar results. For the sake of simplicity, CERES/GEOS p_s was utilized for the main results.

2.3 GPCP Combined Precipitation Dataset

Precipitation P data for this project was derived from the daily Global Precipitation Climatology Project (GPCP daily) Climate Data Record (CDR), Version 1.3 dataset (Huffman et al., 2001; Adler et al., 2018). GPCP combines satellite observations as well as rain gauge data to produce 1^o daily precipitation amount data.

https://doi.org/10.5194/egusphere-2023-2827
Preprint. Discussion started: 4 January 2024

2.4 CALIPSO

The CALIPSO satellite dataset utilized is the AL_LID_L3_Tropospheric_APro_AllSky-Standard-V4-20 dataset (Tackett et al., 2018; Winker, 2019). CALIPSO was utilized to confirm that the mega-fires are associated with an increase in extinction coefficient EC of aerosols, and which atmospheric layers the largest increases in absorbing aerosols are observed. While all other data sets in this study are daily data, CALIPSO only has monthly data available, and this data is at a much coarser resolution (2^o latitude x 5^o longitude). Additionally, CALIPSO only has available data between 2006-2021, while all other utilized datasets have data available from 2003-2022 for the relevant seasonal time frame. For level 3 EC data, CALIPSO distinguishes between 3 types of aerosol: dust, polluted dust, and smoke. This study will primarily utilize the dust and polluted dust EC products.

3 Methods

3.1 Statistics

The bulk of the analysis for this paper involves cumulative distribution functions (CDFs). These CDFs are created by taking a set of data, then fitting a normal distribution. The integral of this normal distribution yields the CDF, which measures the probability of a number, or any number smaller than that number, occurring. Plotting two CDFs on the same axis allows for comparison on how likely an anomaly is to be positive or negative under differing circumstances, such as how likely a positive/negative anomaly for a certain variable is to occur during a high (90th percentile) fire dry matter emission ($DM90$) or low (10th percentile) fire dry matter emission ($DM10$) event. From the calculated normal distributions, effect size of one variable's distribution on another variable's distribution are estimated using Cohen's d d. d is an approximation of by how many standard deviations σs the distribution shifts in response to a change in a variable. In this paper, d is calculated to determine the effect size of DM on other variables. d is approximated using

$$d = \frac{\bar{a} - \bar{b}}{0.5\sqrt{\sigma_a^2 + \sigma_b^2}} \tag{1}$$

where $\bar{a}$ is the mean of the ($DM90$) group (group a), and $\bar{b}$ is the mean of the ($DM10$) group (group b), σ_a is the standard deviation of group a, and σ_b is the standard deviation of group b. d=0.2-0.5 is considered to be a weak effect, d=0.5-0.8 is a moderate effect, and d=0.8 or higher is classified as a strong effect.

When comparing two data sets, a two-tailed pooled t-test is used to assess significance, where the null hypothesis of a zero difference is evaluated, with n_1+n_2-2 degrees of freedom, where n_1 and n_2 are the number of elements in each data set respectively. Here, the pooled variance

$$s^2 = \frac{(n_1 - 1)S_1^2 + (n_2 - 1)S_2^2}{n_1 + n_2 - 2} \tag{2}$$

is used, where S_1 and S_2 are the sample variances. For the purposes of this project, the t-test is evaluated at 90% significance.

https://doi.org/10.5194/egusphere-2023-2827
Preprint. Discussion started: 4 January 2024

3.2 Data Stratification and Comparison

In section 3.1, it was mentioned that CDFs for variable anomalies during anomalously high and low DM emission events are generated to discern to what degree fires impact these anomalies. The purpose of this stratification, particularly stratification of days into anomalously high and low fire events, is to isolate the effects of fires on clouds and/or weather. The remainder of this section will detail how data stratification is accomplished. First, a variable is chosen for analysis (such as CF). Next, this variable as well as the variable(s) that are used to stratify the variable are filtered to include only the region of interest. As the Aqua satellite does not record data for each gridcell at every time step, wherever a coordinate (latitude,longitude,time) is missing a value for a specific variable, the variable(s) it is being stratified by also has the value at that coordinate replaced by a missing value (and vice-versa). Next, to focus on potential feedbacks fires may have on land, a land-sea mask is applied. Then, the daily regional mean for each variable is taken. This is done by first averaging over longitude, then taking a weighted average over latitude. Then, the 2003-2022 wildfire seasons are spliced together, which results in a roughly 3060 day time series. From this 3060 day time series, any days with no data are removed. Next, the average of these time series is removed to give a time series of anomalies for each variable. Then, filters are applied to stratify the variable in question. If the variable is being stratified by one variable (such as DM), the result would be two roughly 306 day long datasets: one stratified by the 90th percentile of the stratification variable, and one stratified by the 10th percentile of the stratification variable. In the cases where the data is stratified by two variables, the result is four datasets. These datasets then have a normal distribution fit to them (Section 3.1) where the average is calculated and a CDF is fit. Once the average is taken for each dataset, σ for each distribution is taken and divided by the square root of the number of data points in each distribution to give the standard error of each dataset. Then, the means can be differentiated from each other to determine if the stratification variable (such as DM) leads to a significant change in the variable anomaly in question. This process can be applied both for a regional average, or on a gridcell-by-gridcell basis. When this process is performed on a gridcell-by-gridcell basis, the Pearson cross correlation coefficient r is determined by spatially correlating the stratified variables with one another. This helps determine if one change in a variable as a result of fires (or other factors) feedbacks onto another to cause a change in anomaly.

3.3 Regions of Interest

First, the region within the southwestern US in which the most significant fire emissions originate from was discerned. Based on what is generally considered to be the time of year in which most wildfires occur in the western US (Urbanski, 2013; Urbanski et al., 2011), data was collected from June 1st-October 31st for the 2003-2022 time frame. 2003-2022 was chosen as this is the time frame in which Aqua satellite data is available for the fire season. Analysis was limited to fire seasons as opposed to the entire year so that the threshold for what constitutes a 90th percentile fire is increased. First, for each gridcell, the 2003-2022 seasonal average daily DM emissions was taken. The portion of the southwestern US that had the largest 2003-2022 seasonal average daily DM emissions is the region that shall be referred to as "northern California" (nCA), which is highlighted in the blue box in **Figure 1a**. The reason for limiting DM data to this region is again to ensure that the threshold for 90th percentile DM is kept high. The nCA region is characterized by temperate forests along the coastline, in the far north,

https://doi.org/10.5194/egusphere-2023-2827
Preprint. Discussion started: 4 January 2024

as well as the east. Agricultural lands are scattered throughout just about every gridcell in nCA, with higher concentrations in the central valley as well as the coastal north. Grasslands are also found throughout most gridcells in this region, with higher concentrations in central CA. The dominant contributor of DM in this region is the temperate forests in the north (**Figure S1**). At this time of year, predominant wind patterns in nCA would favor transportation of smoke from these fires to northern Nevada. During the fire season, northwesterlies tend to blow across nCA towards northern Nevada, and south westerlies blow through the central valley and Sierra Nevada range (Zaremba & Carroll, 1999; LeNoir et al., 1999). Therefore, the expectation is for the majority of wildfire aerosols to be concentrated in nCA, and neighboring northern/central Nevada. In differentiating nCA DM on high fire days and nCA DM on low fire days, AOD is found to be significantly higher in both nCA and Nevada **Figure 1b**, confirming this suspicion. Therefore, from this point forward, the focus will be on the effects of the fires in the blue box in **Figure 1a** (nCA) on the area highlighted in the green box (nCA-NV) in **Figure 1b**.

Figure 1 also serves as a verification of the stratification method, as well as validation of GFED emissions data. Monthly cross correlation analysis (Supplement Section 1) as well as previous works (Wilmot et al., 2022; Schlosser et al., 2017; Cho et al., 2022) indicate that during large fire events, AOD and/or particulate matter concentration are significantly larger compared to no fire conditions. The significant increase in AOD over most of the southwestern US supports the assertion that GFED fire emissions are an acceptable indicator of large fire occurrence.

3.4 CALIPSO

To determine the difference in EC profile between anomalously high and low fire events, the average for each aerosol type's EC at each pressure level was taken over ($DM90$) months and ($DM10$) months in the 2006-2021 range (the time frame in which CALIPSO data is available) in the region of interest. The difference between these two profiles is then taken. The motivation for this process is for one, to remove the effects of potential background aerosols such as BC or OA (from anthropogenic sources such as fossil fuel burning) and isolate the effects of the aerosols emitted from mega-fires. The resulting profile then depicts the effects on the vertical EC profile that fires have. The EC profile of the aerosols is not further stratified as the CALIPSO data is monthly.

4 Results

4.1 Vertical Distribution of Absorbing Aerosols in nCA-NV Region

The three absorbing aerosols that are associated with fires that can be discerned by CALIPSO are smoke, dust, and polluted dust. While dust is not emitted from biomass burning, a number of studies have linked fires to concurrent dust emission through creation of powerful convective updrafts (Wagner et al., 2018, 2021) and delayed dust emissions through wildfire clearing of vegetation (Wagenbrenner et al., 2013, 2017; Yu & Ginoux, 2022). Past observations and modelling experiments have shown dust to create semi-direct effects (Tsikerdekis et al., 2019; Amiri-Farahani et al., 2017; Helmert et al., 2007).

https://doi.org/10.5194/egusphere-2023-2827
Preprint. Discussion started: 4 January 2024

However, increases in non-polluted dust during fires may be related to the concurrence of high winds that tend to be a driver of the mega-fires themselves. Emissions of polluted dust, however, are far more likely to be related to fires, as this aerosol species is a combination of dust and smokey aerosols. Therefore, focus was placed upon smoke and polluted dust. Polluted dust is a mixture of smoke and dust, and therefore should have stronger SW absorption than dust alone. **Figures 2a** & **2b** depict monthly 2006-2021 nCA-NV regional average $EC(DM90)$-$EC(DM10)$ in the daytime (**Figure 2a**) and the nighttime (**Figure 2b**) for both smoke and polluted dust. These plots demonstrate that polluted dust and smoke EC increases significantly in most parts of the troposphere in months where an anomalously large fire occurs. This includes altitudes with pressures p less than 500hPa, where there are relatively large and significant increases in polluted dust (**Figures 2c, 2d**). These high altitude changes are important as in $(DM10)$ months, there is no smoke or polluted dust EC above roughly $p =$400hPa (**Figure S3,S4**), which supports the assertion that wildfire aerosol plumes deposit absorbing aerosols high in the troposphere. However, it should be noted that there are a few altitudes where there is anomalously low smoke EC observed, such as around $p =$900hPa in the daytime profile and around 500-400hPa in the nighttime profile. The standard errors on these negative differences are quite high however, and may be dominated by an outlier month with abnormally high smoke concentration in the $(DM10)$ emission months (possibly from transportation of smoke from a fire outside of the region of interest).

4.2 High & Low Pressure Extremes Stratification

The fingerprints of a semi-direct effect would entail an anomalous warming of the cloud layer, and a corresponding decrease in RH. However, the meteorological conditions around which fires tend to occur need to be taken into account. **Figure 3** depicts cumulative distribution functions (CDFs) for meteorological conditions under high p_s extremes (p_s90) and low p_s extremes (p_s10). High p_s extremes in the southwestern US are associated with higher T throughout the troposphere/surface, reduced RH throughout the troposphere/surface, and reduced CF, while low p_s extremes are associated with the opposite (**Figure 3**). This demonstrates a need to separate the effects of fires from the meteorological effects of high p_s extremes, as positive DM anomalies are significantly more likely to occur on (p_s90) days as opposed to (p_s10) days. Additionally, **Figure 3h** demonstrates that surface wind speeds tend to be larger in the nCA-NV region during p_s10 days. This could impact the transportation of the BB/polluted dust aerosols, potentially allowing for further transportation. **Figure 4a** demonstrates that AOD is not significantly different whether fires occur during (p_s90) or (p_s10) days. However, **Figure 4b,c** demonstrate that the distribution of AOD is significantly different between the positive/negative p_s extremes. Under (p_s90) conditions, the area with the highest AOD is the origin of the BB aerosols: nCA. Under (p_s10) conditions, the AOD is significantly high over both nCA and Nevada.

4.3 Responses in Temperature & Humidity Profiles

The immediate direct effect of BB aerosols tends to be a net cooling of the surface (Sakaeda et al., 2011; Abel et al., 2005). However, semi-direct effects, such as the burning off of low clouds, may overpower this effect, leading to a net surface warming. As the meteorological conditions associated with high pressure days are also hallmarks of a semi-direct effect (**Figure 3**), from here onward data will be stratified into four categories: one with high DM and high p_s ($DM90$,p_s90), one with

https://doi.org/10.5194/egusphere-2023-2827
Preprint. Discussion started: 4 January 2024

low DM and high p_s ($DM10$,p_s90), one with high DM and low p_s ($DM90$,p_s10), and one with one with low DM and low p_s ($DM10$,p_s10). In differentiating the average of the variables on ($DM90$,p_s90) days and ($DM10$,p_s90) days, the effects of fires can be discerned independent of the meteorological conditions that come with high p_s extremes. Additionally, in comparing the ($DM90$,p_s10) dataset to the ($DM10$,p_s10) dataset, the effects of high p_s are not present, so this further isolates the effects of the fires. **Figure 5** displays 2003-2022 June-October nCA-NV vertical profiles of high minus low fire days' T (**Figure 5a,d** and RH (**Figure 5c,f**) profiles. **Figure 5a-c** are stratified by high p_s, while **Figure 5d-f** are stratified by low p_s. These profiles demonstrate that when anomalously large fires are occurring, whether it is during high or low pressure extremes, temperature is significantly anomalously high at all points of the troposphere at $p \geq$250hPa compared to conditions with anomalously low fires. In both **Figure 5a** and **Figure 5d**, the temperatures in the 850hPa to 250hPa pressure level range are consistently significantly higher than the surface layer (900hPa to 1000hPa). Comparing **Figure 5** to **Figure 2**, the positive differences in temperature anomaly are generally consistent with the positive differences in polluted dust and/or smoke EC. In comparing **Figure 5d** to **Figure 5c**, RH anomalies in the 700hPa to 250hPa range (and at sea level) are significantly lower when anomalously large fires occur during low pressure extremes.

Aside from temperature, the other potential factor that could affect RH is that of specific humidity, which is analogous to water mass mixing ratio M_{H_2O}. Utilizing the same process that generated the T and RH profiles, profiles of M_{H_2O} were generated for high and low p_s extremes (**Figures 5b,e**). There is no significant anomaly under high p_s conditions, but under low p_s there are significant negative anomalies at 1000hPa, and 500-300hPa. This means that the negative RH anomaly in the high troposphere under high fire conditions is due at least in part to a negative specific humidity anomaly. **Figure 6** depicts high minus low DM extremes' 500hPa-250hPa and 700hPa-500hPa T, M_{H_2O}, and RH anomalies during low p_s extremes. In both the high and low/mid-troposphere in the nCA-NV region (highlighted in the green box), there are significant increases in T and decreases in RH. However, in the high troposphere, there is a significant decrease in M_{H_2O} over Nevada that is not present in the low/mid troposphere. Therefore, decreases in RH in the high troposphere are likely in part due to changes in M_{H_2O} in addition to increases in T. It is unknown if the fires are the cause of this difference in specific humidity anomaly, but this is further explored in section 2 of the supplement. As the change in T is the more robust signal over all parts of the troposphere, the changes in T will be the focus of the remainder of the paper.

4.4 Changes in Cloud Fraction, Precipitation, and Shortwave Flux

Figure 5 implies that during anomalously large fire events, there is a significant increase in temperatures in the low, mid, and high troposphere compared to anomalously low fire conditions. Does this increase in temperature translate to a decrease in CF, and therefore a change in the radiative balance? **Figure 7** displays CDFs for nCA-NV regional average variable anomalies during high DM/low p_s days (solid red), low DM/high p_s days (dashed red), high DM/low p_s days (solid blue), and low DM/low p_s days (dashed blue). **Figure 7a** and **Figure 7b** demonstrate that during both high and low p_s extreme days, the mean liquid water cloud fraction CF_{lw} anomaly and cirrus cloud fraction anomaly CF_{cir} anomaly are shifted significantly leftward under high DM conditions. This implies that when anomalously large fires occur, there is a significantly higher probability

https://doi.org/10.5194/egusphere-2023-2827
Preprint. Discussion started: 4 January 2024

(at the 90% confidence interval) of seeing a negative CF_{lw} and/or CF_{cir} anomaly. While the distribution of all other variables depicted in **Figure 7**, such as CF, cloud top height CTH, P, and outgoing top of atmosphere shortwave flux $TOA\ SW$ flux, are shifted leftward on high DM days compared to low DM days, the shifts are not significant during high p_s extremes. However, these shifts are significant for low p_s extreme days (**Figure 7**). The explanation for as to why the distribution shifts farther leftward when anomalously large fires occur during low pressure compared to high pressure extremes lies in **Figure 5**. High pressure extremes create conditions favorable for sinking air. During high pressure extremes, RH is already significantly lower than normal conditions, as temperatures throughout the troposphere are already high and atmospheric water vapor content is low. This creates conditions of cloud-free skies. Therefore, further decreasing the already low RH should not lead to significantly lower cloud fraction, P, or outgoing $TOA\ SW$ flux as CF is already low. However, during low DM/low p_s days, **Figure 7** demonstrates that conditions are favorable for clouds and rain. This is because during these low pressure extremes, T is lower and RH is high. Therefore, when anomalously large fires introduce aerosols that create a semi-direct effect, the drop in RH is significant enough to reduce the chances of seeing positive cloud/rain anomalies. In response to the higher probability of negative cloud fraction anomaly, the probability that SW radiation will be reflected back into space decreases. The effect sizes of high DM emissions on nCA-NV regional averages of the variables in **Figure 7** are depicted in **Figure 8**. **Figure 8a** demonstrates that during high p_s extremes, anomalously large fires have a weak-to-no effect size on the relevant variables. For low p_s extremes, the anomalously large fires have a moderate-to-strong effect size on the relevant variables.

Thus far, the focus of this project has been on the regional average of the nCA-NV region. However, it is essential to determine if the changes in the relevant variables are spatially consistent. As the fire semi-direct effect signal is strongest during significant low pressure days, the focus from here will be on the meteorological effects of fires during high DM/low p_s days. **Figure 9** displays composite differences between high DM/low p_s and low DM/low p_s days' meteorological variables for each gridcell over the entire southwestern US. **Figures 6a,b** display the composite differences in cloud layer (700hPa$\geq p \geq$250hPa) temperature T_{CL} and cloud layer relative humidity RH_{CL}. These plots depict that T_{CL} significantly (significant changes are marked with a black dot in each gridcell) increases almost everywhere across California and Nevada, with the most significant increase in the green box (the nCA-NV region). The differences in T_{CL} correlate significantly with $AOD(DM90$,$p_s10)$-$AOD(DM10$,$p_s10)$ at $r = 0.79$ across the entire southwest. The decreases in RH_{CL} have a very similar spatial distribution to T_{CL}, with the strongest decreases in the nCA-NV region. Again, this correlates significantly with AOD with $r = -0.77$ over the entire southwest. While the increases in cloud layer T are widespread across all of California and Nevada, significant increases in T_s (**Figure 9c**), decreases in RH_s (**Figure 9d**), decreases in CF (**Figure 9e**), decreases in CTH (**Figure 9f**), decreases in P (**Figure 9g**), and decreases in $TOA\ SW$ flux (**Figure 9h**) are essentially exclusive to the nCA-NV region. The differences in all of these variables across the southwestern US correlate significantly with AOD, supporting the assertion that aerosols concurrent with fires create semi-direct effects. Of particular note are the changes in T_s and P, which are two variables intrinsically related to fire duration. A spatial cross correlation of the change in T_s and $TOA\ SW$ yields r =-0.59, which is significant at the 90% confidence interval. Furthermore, correlating P with RH_{CL} using the same method yields an even stronger correlation of r =0.80. Breaking down the changes in CF into liquid and ice cloud components, it appears that

https://doi.org/10.5194/egusphere-2023-2827
Preprint. Discussion started: 4 January 2024

cirrus clouds contribute the most to the decrease in CF and CTH. **Figure 10** depicts composite differences between high DM/low p_s and low DM/low p_s days' CF_{lw} and CF_{cir}. The differences in CF_{lw} are spatially consistent with the changes in RH in the 700-500hPa levels of the troposphere, while The differences in CF_{cir} are spatially consistent with the changes in RH in the 500-200hPa levels of the troposphere (**Figure 6**).

4.5 Cloud Microphysical Effects

Up to this point, we have investigated aerosol direct/semi-direct effects on clouds. Aerosols may also influence clouds via microphysical effects, which are investigated in this section. High fire emissions under both low and high p_s conditions are associated with non-significant differences in liquid and ice R_{eff} (**Figure 11**). Under high fire/high p_s extremes, there is an increase in ice water path IWP. IWP scales positively with T, so this is a fingerprint of a dominate radiative effect (Ou & Liou, 1995). Furthermore, there is a significant decrease in LWP under anomalously high fire/low p_s conditions. This significant decrease in LWP may be due to the decrease in RH, which reduces liquid water within clouds. This decrease in LWP may be of importance, as LWP scales positively with cloud albedo (Han et al., 1998). Therefore, this decrease in LWP may contribute to an increase in absorbed solar radiation at the surface. In summary, while the nCA fires significantly inject of aerosols into the troposphere, these aerosols do not appear to act as CCN, and instead burn off clouds. Previously, BC has been shown to aid cloud droplet/ice formation, but only after the particles have undergone over a week of aging (Lohmann et al., 2020). Therefore, the freshly emitted BC during the anomalously high fire events may be too hydrophobic to act as CCN, and instead radiative effects of the aerosol dominate. Additionally, the warming effects of these aerosols may reduce RH to the point where clouds are unable to form in the first place.

5 Discussion

The results of this paper indicate that large fires in nCA are concurrent with significant amounts of absorbing aerosols and a warmer troposphere. When the fires occur during low p_s extremes, this increase in T is associated with a significant decrease in RH in the low, mid, and high cloud layers (700hPa-250hPa) at the 90% confidence interval. This decrease in RH is associated with a reduction of clouds, which results in a reduction in CF and P significantly in the nCA-NV region. This reduction in clouds is then associated with a reduction in outgoing $TOA\ SW$ flux. This reduction in outgoing $TOA\ SW$ flux is concurrent with an increase in T_s and a reduction in RH_s in the nCA-NV region. However, this warming effect may be somewhat muted by a reduction in CTH, which could increase outgoing TOA LW flux, presumably as a result of a disproportionate reduction in CF_{cir} compared to CF_{lw} seen in **Figure 9**. In short, during low pressure extremes, fires in nCA appear to create a positive feedback that entails emissions of absorbing aerosols that warm the troposphere, creating a semi-direct effect. This semi-direct effect then creates conditions more favorable to fires, including warmer surface temperatures and reduced P, as a result of reduced cloud cover and cloud layer RH. Significant reductions in nCA P may prolong the wildfire season further into autumn (Goss et al., 2020), and increases in T_s as well as decreases in RH_s may create conditions more favorable for more fires to ignite and grow. This positive feedback may also prolong poor air quality conditions inside the southwestern

https://doi.org/10.5194/egusphere-2023-2827
Preprint. Discussion started: 4 January 2024

US (Liu & Peng, 2019; O'Neill et al., 2021; Schlosser et al., 2017), as well as other parts of the country (Hung et al., 2020). Additionally, these significant decreases in P and/or increases T_s occur in heavily populated regions in the southwestern US, including: the San Francisco bay area, Humboldt County in California, and Washoe County in Nevada. It is possible that these results may also be applicable to other Mediterranean climates, but further research is needed. Therefore, this study highlights an increased need for a curtailment of CO_2 emissions (Ma et al., 2021; Touma et al., 2021) and better land management practices (DellaSala et al., 2022; Minnich et al., 2000; Minnich, 2001), as climate change and land mismanagement have both contributed to the mega-fires in nCA in recent years. Additionally, this paper highlights the need for more climate models to incorporate feedbacks between wildfires, their aerosols, and semi-direct effects. Models that include interactive emissions of BB aerosols as well as account for the radiative effects of these aerosols on the surface are few and far between, and those that do exist remain in their infancy (Mangeon et al., 2016; Li et al., 2012). Furthermore, as the fire module of these models tend to be unused in the main CMIP simulations, this study highlights a potential deficiency in projections of radiative balance, fire lifetime, and the corresponding air quality impacts in climate model simulations. Therefore, future projections of fire duration, and the associated air quality reduction may be underestimated.

Code availability. Code used to process satellite data is available upon request from author.

Data availability. All datasets utilized in this analysis are available online. MODIS datasets are available via the 787 NASA Level-1 and Atmosphere Archive & Distribution System (LAADS) Distributed Active Archive 788 Center (DAAC) at https://ladsweb.modaps.eosdis.nasa.gov/archive/allData/61/. CERES datasets can be found at https://ceres.larc.nasa.gov/. AIRS data is available via NASA's Earth Science Data 794 extremes (ESDS) program at https://www.earthdata.nasa.gov/. CALIPSO datasets are available at the Atmospheric Science Data Center (ASDC) at https://asdc.larc.nasa.gov/. GFED fire emission data is archived on the GFED web page at https://www.globalfiredata.org/. MERRA-2 data can be found on the Goddard Earth Sciences Data and Information Services Center (GES DISC) website at https://disc.gsfc.nasa.gov/datasets?project=MERRA-2.

https://doi.org/10.5194/egusphere-2023-2827
Preprint. Discussion started: 4 January 2024

Appendix A

Symbol	Definition	Dataset Derived From	Name of Product Used
DM	Fire dry matter emissions	GFED	DM, daily_fraction
p_s	Surface Pressure	CERES/GEOS	sfc_press
AOD	Aerosol Optical Depth	MODIS Deep Blue	Deep_Blue_Aerosol_Optical_Depth_550_Land_Mean
M_{H_2O}	Water Mass Mixing Ratio	AIRS	H2O_MMR_D
EC	Extinction Coefficient	CALIPSO	Extinction_Coefficient_532_Mean_Elevated_Smoke, Extinction_Coefficient_532_Mean_Polluted_Dust Extinction_Coefficient_532_Mean_Dust
T	Temperature	AIRS	Temperature_D
T_s	Surface Temperature	AIRS	SurfAirTemp_D
RH	Relative Humidity	AIRS	RelHum_D
RH_s	Surface Relative Humidity	AIRS	RelHumSurf_D
CF	Cloud Fraction	MODIS	Cloud_Fraction_Mean
CF_{cir}	Cirrus Cloud Fraction	MODIS	Cirrus_Fraction_Infrared
CF_{lw}	Liquid Water Cloud Fraction	MODIS	Cloud_Retrieval_Fraction_Liquid
CTH	Cloud Top Height	MODIS	Cloud_Top_Height_Mean
P	Precipitation	GPCP	precip
$TOA\ SW$	Outgoing Top of Atmosphere Short Wave Flux	CERES	all_toa_sw
U_s	Surface Wind speed	CERES/GEOS	sfc_wind_speed
Liquid R_{eff}	Liquid Cloud Effective Radius	MODIS	Cloud_Effective_Radius_Ice_Mean
Ice R_{eff}	Ice Cloud Effective Radius	MODIS	Cloud_Effective_Radius_Liquid_Mean
LWP	Liquid Water Path	MODIS	Cloud_Water_Path_Liquid_Mean
IWP	Ice Water Path	MODIS	Cloud_Water_Path_Ice_Mean

Table A1. Definition of variables that were derived from satellite observational datasets, as well as the instrument and dataset they are derived from.

https://doi.org/10.5194/egusphere-2023-2827
Preprint. Discussion started: 4 January 2024

Symbol	Definition
nCA	Northern California
nCA-NV	Northern California-Nevada
US	United States
BB	Biomass Burning
BC	Black Carbon
OA	Organic Aerosol
CA	California
SW	Shortwave
AAOD	Absorbing Aerosol Optical Depth
LW	Longwave
CCN	Cloud Condensation Nuclei
CDF	Cumulative Distribution Function

Table A2. Definitions of abbreviations found throughout the paper that are not associated with a dataset.

https://doi.org/10.5194/egusphere-2023-2827
Preprint. Discussion started: 4 January 2024

Descriptor	Definition
$(DM90)$	Variable stratified by 90th percentile fire dry matter emission anomaly days in nCA
(p_s90)	Variable stratified by 90th percentile surface pressure anomaly days in nCA-NV
$(DM10)$	Variable stratified by 10th percentile fire dry matter emission anomaly days in nCA
(p_s10)	Variable stratified by 10th percentile surface pressure anomaly days in nCA-NV
$(DM90, p_s90)$	Variable stratified by 90th percentile fire dry matter emission anomaly days in nCA and 90th percentile surface pressure anomaly days in nCA-NV
$(DM10, p_s90)$	Variable stratified by 10th percentile fire dry matter emission anomaly days in nCA and 90th percentile surface pressure anomaly days in nCA-NV
$(DM90, p_s10)$	Variable stratified by 90th percentile fire dry matter emission anomaly days in nCA and 10th percentile surface pressure anomaly days in nCA-NV
$(DM10, p_s10)$	Variable stratified by 10th percentile fire dry matter emission anomaly days in nCA and 10th percentile surface pressure anomaly days in nCA-NV
cl	Cloud layer (700-250hPa) average of variable
s	Variable measured at the surface
ht	High troposphere (500-200hPa) average of variable
lt	Low/mid Troposphere (700-500hPa) average of variable
Δ	Difference in variable under different fire and/or pressure conditions

Table A3. Definitions of subscripts and other descriptors for variables.

375 *Author contributions.* J.L.G. conceived the project, designed the study, performed data analysis and wrote the paper. R.J.A. performed analyses, and wrote the paper. K.L. advised on methods.

Competing interests. The authors declare no competing interests.

https://doi.org/10.5194/egusphere-2023-2827
Preprint. Discussion started: 4 January 2024

Acknowledgements. R.J. Allen is supported by NSF grant AGS-2153486.

https://doi.org/10.5194/egusphere-2023-2827
Preprint. Discussion started: 4 January 2024

References

Abel, S. J., Highwood, E. J., Haywood, J. M., & Stringer, M. A. (2005). The direct radiative effect of biomass burning aerosols over southern Africa. *Atmospheric Chemistry and Physics*, 5(7), 1999–2018. Publisher: Copernicus GmbH.

Adler, R. F., Sapiano, M. R. P., Huffman, G. J., Wang, J.-J., Gu, G., Bolvin, D., Chiu, L., Schneider, U., Becker, A., Nelkin, E., Xie, P., Ferraro, R., & Shin, D.-B. (2018). The Global Precipitation Climatology Project (GPCP) Monthly Analysis (New Version 2.3) and a Review of 2017 Global Precipitation. *Atmosphere*, 9(4), 138.

Ager, A. A., Day, M. A., Alcasena, F. J., Evers, C. R., Short, K. C., & Grenfell, I. (2021). Predicting Paradise: Modeling future wildfire disasters in the western US. *Science of The Total Environment*, 784, 147057.

AIRS Science Team & Texeira, J. (2013). Aqua AIRS Level 3 Standard Daily Product using AIRS IR-only V6.

Allen, R. J., Hassan, T., Randles, C. A., & Su, H. (2019). Enhanced land–sea warming contrast elevates aerosol pollution in a warmer world. *Nature Climate Change*, 9(4), 300–305.

Allen, R. J. & Sherwood, S. C. (2010). Aerosol-cloud semi-direct effect and land-sea temperature contrast in a GCM. *Geophysical Research Letters*, 37(7). _eprint: https://onlinelibrary.wiley.com/doi/pdf/10.1029/2010GL042759.

Allen, R. J., Zhao, X., Randles, C. A., Kramer, R. J., Samset, B. H., & Smith, C. J. (2023). Surface warming and wetting due to methane's long-wave radiative effects muted by short-wave absorption. *Nature Geoscience*, 16(4), 314–320. Number: 4 Publisher: Nature Publishing Group.

Amiri-Farahani, A., Allen, R. J., Li, K.-F., Nabat, P., & Westervelt, D. M. (2020). A La Niña-Like Climate Response to South African Biomass Burning Aerosol in CESM Simulations. *Journal of Geophysical Research: Atmospheres*, 125(6), e2019JD031832.

Amiri-Farahani, A., Allen, R. J., Neubauer, D., & Lohmann, U. (2017). Impact of Saharan dust on North Atlantic marine stratocumulus clouds: importance of the semidirect effect. *Atmospheric Chemistry and Physics*, 17(10), 6305–6322. Publisher: Copernicus GmbH.

Brown, P. T., Hanley, H., Mahesh, A., Reed, C., Strenfel, S. J., Davis, S. J., Kochanski, A. K., & Clements, C. B. (2023). Climate warming increases extreme daily wildfire growth risk in California. *Nature*, (pp. 1–7). Publisher: Nature Publishing Group.

Cape, J. N., Coyle, M., & Dumitrean, P. (2012). The atmospheric lifetime of black carbon. *Atmospheric Environment*, 59, 256–263.

Cho, C., Kim, S.-W., Choi, W., & Kim, M.-H. (2022). Significant light absorption of brown carbon during the 2020 California wildfires. *Science of The Total Environment*, 813, 152453.

DellaSala, D. A., Baker, B. C., Hanson, C. T., Ruediger, L., & Baker, W. (2022). Have western USA fire suppression and megafire active management approaches become a contemporary Sisyphus? *Biological Conservation*, 268, 109499.

Doelling, D. (2016). CERES Level 3 SSF1deg-Day Aqua-MODIS HDF file - Edition 4A.

Eyring, V., Bony, S., Meehl, G. A., Senior, C. A., Stevens, B., Stouffer, R. J., & Taylor, K. E. (2016). Overview of the Coupled Model Intercomparison Project Phase 6 (CMIP6) experimental design and organization. *Geoscientific Model Development*, 9(5), 1937–1958.

Fasullo, J. T., Rosenbloom, N., Buchholz, R. R., Danabasoglu, G., Lawrence, D. M., & Lamarque, J.-F. (2021). Coupled Climate Responses to Recent Australian Wildfire and COVID-19 Emissions Anomalies Estimated in CESM2. *Geophysical Research Letters*, 48(15), e2021GL093841. _eprint: https://onlinelibrary.wiley.com/doi/pdf/10.1029/2021GL093841.

Giglio, L., Randerson, J. T., & van der Werf, G. R. (2013). Analysis of daily, monthly, and annual burned area using the fourth-generation global fire emissions database (GFED4). *Journal of Geophysical Research: Biogeosciences*, 118(1), 317–328. _eprint: https://onlinelibrary.wiley.com/doi/pdf/10.1002/jgrg.20042.

Gomez, J., Allen, R. J., Turnock, S. T., Horowitz, L. W., Tsigaridis, K., Bauer, S. E., Olivié, D., Thomson, E. S., & Ginoux, P. (2023). The projected future degradation in air quality is caused by more abundant natural aerosols in a warmer world. *Communications Earth & Environment*, 4(1), 1–11. Number: 1 Publisher: Nature Publishing Group.

Goss, M., Swain, D. L., Abatzoglou, J. T., Sarhadi, A., Kolden, C. A., Williams, A. P., & Diffenbaugh, N. S. (2020). Climate change is increasing the likelihood of extreme autumn wildfire conditions across California. *Environmental Research Letters*, 15(9), 094016. Publisher: IOP Publishing.

Han, Q., Rossow, W. B., Chou, J., & Welch, R. M. (1998). Global Survey of the Relationships of Cloud Albedo and Liquid Water Path with Droplet Size Using ISCCP. *Journal of Climate*, 11(7), 1516–1528. Publisher: American Meteorological Society Section: Journal of Climate.

Helmert, J., Heinold, B., Tegen, I., Hellmuth, O., & Wendisch, M. (2007). On the direct and semidirect effects of Saharan dust over Europe: A modeling study. *Journal of Geophysical Research: Atmospheres*, 112(D13). _eprint: https://onlinelibrary.wiley.com/doi/pdf/10.1029/2006JD007444.

Herbert, R. & Stier, P. (2023). Satellite observations of smoke–cloud–radiation interactions over the Amazon rainforest. *Atmospheric Chemistry and Physics*, 23(7), 4595–4616. Publisher: Copernicus GmbH.

Highwood, E. J. & Ryder, C. L. (2014). Radiative Effects of Dust. In P. Knippertz & J.-B. W. Stuut (Eds.), *Mineral Dust: A Key Player in the Earth System* (pp. 267–286). Dordrecht: Springer Netherlands.

Huffman, G. J., Adler, R. F., Morrissey, M. M., Bolvin, D. T., Curtis, S., Joyce, R., McGavock, B., & Susskind, J. (2001). Global Precipitation at One-Degree Daily Resolution from Multisatellite Observations. *Journal of Hydrometeorology*, 2(1), 36–50.

Hung, W.-T., Lu, C.-H. S., Shrestha, B., Lin, H.-C., Lin, C.-A., Grogan, D., Hong, J., Ahmadov, R., James, E., & Joseph, E. (2020). The impacts of transported wildfire smoke aerosols on surface air quality in New York State: A case study in summer 2018. *Atmospheric Environment*, 227, 117415.

Keeley, J. E. & Syphard, A. D. (2019). Twenty-first century California, USA, wildfires: fuel-dominated vs. wind-dominated fires. *Fire Ecology*, 15(1), 24.

Koch, D. & Del Genio, A. D. (2010). Black carbon semi-direct effects on cloud cover: review and synthesis. *Atmospheric Chemistry and Physics*, 10(16), 7685–7696.

LeNoir, J. S., McConnell, L. L., Fellers, G. M., Cahill, T. M., & Seiber, J. N. (1999). Summertime transport of current-use pesticides from California's Central Valley to the Sierra Nevada Mountain Range, USA. *Environmental Toxicology and Chemistry*, 18(12), 2715–2722. _eprint: https://onlinelibrary.wiley.com/doi/pdf/10.1002/etc.5620181210.

Levy, R. C., Mattoo, S., Munchak, L. A., Remer, L. A., Sayer, A. M., Patadia, F., & Hsu, N. C. (2013). The Collection 6 MODIS aerosol products over land and ocean. *Atmospheric Measurement Techniques*, 6(11), 2989–3034.

Li, F., Zeng, X. D., & Levis, S. (2012). A process-based fire parameterization of intermediate complexity in a Dynamic Global Vegetation Model. *Biogeosciences*, 9(7), 2761–2780. Publisher: Copernicus GmbH.

Li, S. & Banerjee, T. (2021). Spatial and temporal pattern of wildfires in California from 2000 to 2019. *Scientific Reports*, 11(1), 8779.

Liu, J. C. & Peng, R. D. (2019). The impact of wildfire smoke on compositions of fine particulate matter by ecoregion in the Western US. *Journal of Exposure Science & Environmental Epidemiology*, 29(6), 765–776. Number: 6 Publisher: Nature Publishing Group.

Lohmann, U., Friebel, F., Kanji, Z. A., Mahrt, F., Mensah, A. A., & Neubauer, D. (2020). Future warming exacerbated by aged-soot effect on cloud formation. *Nature Geoscience*, 13(10), 674–680. Number: 10 Publisher: Nature Publishing Group.

https://doi.org/10.5194/egusphere-2023-2827
Preprint. Discussion started: 4 January 2024

Ma, W., Zhai, L., Pivovaroff, A., Shuman, J., Buotte, P., Ding, J., Christoffersen, B., Knox, R., Moritz, M., Fisher, R. A., Koven, C. D., Kueppers, L., & Xu, C. (2021). Assessing climate change impacts on live fuel moisture and wildfire risk using a hydrodynamic vegetation model. *Biogeosciences*, 18(13), 4005–4020. Publisher: Copernicus GmbH.

Mangeon, S., Voulgarakis, A., Gilham, R., Harper, A., Sitch, S., & Folberth, G. (2016). INFERNO: a fire and emissions scheme for the UK Met Office's Unified Model. *Geoscientific Model Development*, 9(8), 2685–2700.

Minnich, R. A. (2001). An Integrated Model of Two Fire Regimes. *Conservation Biology*, 15(6), 1549–1553.

Minnich, R. A., Barbour, M. G., Burk, J. H., & Sosa-Ramírez, J. (2000). Californian mixed-conifer forests under unmanaged fire regimes in the Sierra San Pedro Mártir, Baja California, Mexico. *Journal of Biogeography*, 27(1), 105–129. _eprint: https://onlinelibrary.wiley.com/doi/pdf/10.1046/j.1365-2699.2000.00368.x.

MODIS Atmosphere Science Team (2017). MYD08_d3 MODIS/Aqua Aerosol Cloud Water Vapor Ozone Daily L3 Global 1Deg CMG.

Ou, S.-c. & Liou, K.-N. (1995). Ice microphysics and climatic temperature feedback. *Atmospheric Research*, 35(2), 127–138.

O'Neill, S. M., Diao, M., Raffuse, S., Al-Hamdan, M., Barik, M., Jia, Y., Reid, S., Zou, Y., Tong, D., West, J. J., Wilkins, J., Marsha, A., Freedman, F., Vargo, J., Larkin, N. K., Alvarado, E., & Loesche, P. (2021). A multi-analysis approach for estimating regional health impacts from the 2017 Northern California wildfires. *Journal of the Air & Waste Management Association*, 71(7), 791–814.

Palinkas, L. A. (2020). The California Wildfires. In L. A. Palinkas (Ed.), *Global Climate Change, Population Displacement, and Public Health: The Next Wave of Migration* (pp. 53–67). Cham: Springer International Publishing.

Platnick, S., King, M., Ackerman, S., Menzel, W., Baum, B., Riedi, J., & Frey, R. (2003). The MODIS cloud products: algorithms and examples from Terra. *IEEE Transactions on Geoscience and Remote Sensing*, 41(2), 459–473. Conference Name: IEEE Transactions on Geoscience and Remote Sensing.

Platnick, S., Meyer, K. G., King, M. D., Wind, G., Amarasinghe, N., Marchant, B., Arnold, G. T., Zhang, Z., Hubanks, P. A., Holz, R. E., Yang, P., Ridgway, W. L., & Riedi, J. (2017). The MODIS Cloud Optical and Microphysical Products: Collection 6 Updates and Examples From Terra and Aqua. *IEEE Transactions on Geoscience and Remote Sensing*, 55(1), 502–525.

Randerson, J., van der Werf, G., Giglio, L., Collatz, G., & Kasibhatla, P. (2017). Global Fire Emissions Database, Version 4.1 (GFEDv4). (pp. 1925.7122549999906 MB). Artwork Size: 1925.7122549999906 MB Publisher: ORNL Distributed Active Archive Center.

Sakaeda, N., Wood, R., & Rasch, P. J. (2011). Direct and semidirect aerosol effects of southern African biomass burning aerosol. *Journal of Geophysical Research: Atmospheres*, 116(D12). _eprint: https://onlinelibrary.wiley.com/doi/pdf/10.1029/2010JD015540.

Salomonson, V., Barnes, W., Xiong, J., Kempler, S., & Masuoka, E. (2002). An overview of the Earth Observing System MODIS instrument and associated data systems performance. In *IEEE International Geoscience and Remote Sensing Symposium*, volume 2 (pp. 1174–1176 vol.2).

Schlosser, J. S., Braun, R. A., Bradley, T., Dadashazar, H., MacDonald, A. B., Aldhaif, A. A., Aghdam, M. A., Mardi, A. H., Xian, P., & Sorooshian, A. (2017). Analysis of aerosol composition data for western United States wildfires between 2005 and 2015: Dust emissions, chloride depletion, and most enhanced aerosol constituents. *Journal of Geophysical Research: Atmospheres*, 122(16), 8951–8966.

Smith, C. J., Kramer, R. J., Myhre, G., Forster, P. M., Soden, B. J., Andrews, T., Boucher, O., Faluvegi, G., Fläschner, D., Hodnebrog, Ø., Kasoar, M., Kharin, V., Kirkevåg, A., Lamarque, J.-F., Mülmenstädt, J., Olivié, D., Richardson, T., Samset, B. H., Shindell, D., Stier, P., Takemura, T., Voulgarakis, A., & Watson-Parris, D. (2018). Understanding Rapid Adjustments to Diverse Forcing Agents. *Geophysical Research Letters*, 45(21), 12,023–12,031. _eprint: https://onlinelibrary.wiley.com/doi/pdf/10.1029/2018GL079826.

Stjern, C. W., Samset, B. H., Myhre, G., Forster, P. M., Hodnebrog, Ø., Andrews, T., Boucher, O., Faluvegi, G., Iversen, T., Kasoar, M., Kharin, V., Kirkevåg, A., Lamarque, J.-F., Olivié, D., Richardson, T., Shawki, D., Shindell, D., Smith, C. J., Takemura, T., & Voulgarakis,

A. (2017). Rapid Adjustments Cause Weak Surface Temperature Response to Increased Black Carbon Concentrations. *Journal of Geophysical Research: Atmospheres*, 122(21), 11,462–11,481. _eprint: https://onlinelibrary.wiley.com/doi/pdf/10.1002/2017JD027326.

Tackett, J. L., Winker, D. M., Getzewich, B. J., Vaughan, M. A., Young, S. A., & Kar, J. (2018). CALIPSO lidar level 3 aerosol profile product: version 3 algorithm design. *Atmospheric Measurement Techniques*, 11(7), 4129–4152.

Touma, D., Stevenson, S., Lehner, F., & Coats, S. (2021). Human-driven greenhouse gas and aerosol emissions cause distinct regional impacts on extreme fire weather. *Nature Communications*, 12(1), 212.

Tsikerdekis, A., Zanis, P., Georgoulias, A. K., Alexandri, G., Katragkou, E., Karacostas, T., & Solmon, F. (2019). Direct and semi-direct radiative effect of North African dust in present and future regional climate simulations. *Climate Dynamics*, 53(7), 4311–4336.

Twohy, C. H., Toohey, D. W., Levin, E. J. T., DeMott, P. J., Rainwater, B., Garofalo, L. A., Pothier, M. A., Farmer, D. K., Kreidenweis, S. M., Pokhrel, R. P., Murphy, S. M., Reeves, J. M., Moore, K. A., & Fischer, E. V. (2021). Biomass Burning Smoke and Its Influence on Clouds Over the Western U. S. *Geophysical Research Letters*, 48(15), e2021GL094224.

United Nations Environment Programme (2022). Spreading like Wildfire – The Rising Threat of Extraordinary Landscape Fires.

Urbanski, S. P. (2013). Combustion efficiency and emission factors for wildfire-season fires in mixed conifer forests of the northern Rocky Mountains, US. *Atmospheric Chemistry and Physics*, 13(14), 7241–7262.

Urbanski, S. P., Hao, W. M., & Nordgren, B. (2011). The wildland fire emission inventory: western United States emission estimates and an evaluation of uncertainty. *Atmospheric Chemistry and Physics*, 11(24), 12973–13000.

van der Werf, G. R., Randerson, J. T., Giglio, L., van Leeuwen, T. T., Chen, Y., Rogers, B. M., Mu, M., van Marle, M. J. E., Morton, D. C., Collatz, G. J., Yokelson, R. J., & Kasibhatla, P. S. (2017). Global fire emissions estimates during 1997–2016. *Earth System Science Data*, 9(2), 697–720.

Varga, K., Jones, C., Trugman, A., Carvalho, L. M. V., McLoughlin, N., Seto, D., Thompson, C., & Daum, K. (2022). Megafires in a Warming World: What Wildfire Risk Factors Led to California's Largest Recorded Wildfire. *Fire*, 5(1), 16. Number: 1 Publisher: Multidisciplinary Digital Publishing Institute.

Wagenbrenner, N. S., Chung, S. H., & Lamb, B. K. (2017). A large source of dust missing in Particulate Matter emission inventories? Wind erosion of post-fire landscapes. *Elementa: Science of the Anthropocene*, 5, 2.

Wagenbrenner, N. S., Germino, M. J., Lamb, B. K., Robichaud, P. R., & Foltz, R. B. (2013). Wind erosion from a sagebrush steppe burned by wildfire: Measurements of PM10 and total horizontal sediment flux. *Aeolian Research*, 10, 25–36.

Wagner, R., Jähn, M., & Schepanski, K. (2018). Wildfires as a source of airborne mineral dust – revisiting a conceptual model using large-eddy simulation (LES). *Atmospheric Chemistry and Physics*, 18(16), 11863–11884.

Wagner, R., Schepanski, K., & Klose, M. (2021). The Dust Emission Potential of Agricultural-Like Fires—Theoretical Estimates From Two Conceptually Different Dust Emission Parameterizations. *Journal of Geophysical Research: Atmospheres*, 126(18), e2020JD034355. _eprint: https://onlinelibrary.wiley.com/doi/pdf/10.1029/2020JD034355.

Wei, J., Li, Z., Peng, Y., & Sun, L. (2019). MODIS Collection 6.1 aerosol optical depth products over land and ocean: validation and comparison. *Atmospheric Environment*, 201, 428–440.

Wielicki, B., Barkstrom, B., Baum, B., Charlock, T., Green, R., Kratz, D., Lee, R., Minnis, P., Smith, G., Wong, T., Young, D., Cess, R., Coakley, J., Crommelynck, D., Donner, L., Kandel, R., King, M., Miller, A., Ramanathan, V., Randall, D., Stowe, L., & Welch, R. (1998). Clouds and the Earth's Radiant Energy System (CERES): algorithm overview. *IEEE Transactions on Geoscience and Remote Sensing*, 36(4), 1127–1141. Conference Name: IEEE Transactions on Geoscience and Remote Sensing.

https://doi.org/10.5194/egusphere-2023-2827
Preprint. Discussion started: 4 January 2024

Wilmot, T. Y., Mallia, D. V., Hallar, A. G., & Lin, J. C. (2022). Wildfire plumes in the Western US are reaching greater heights and injecting more aerosols aloft as wildfire activity intensifies. *Scientific Reports*, 12(1), 12400. Number: 1 Publisher: Nature Publishing Group.

Winker, D. (2019). CALIPSO Lidar Level 3 Tropospheric Aerosol Profiles, All Sky Data, Standard V4-20.

530 Yu, Y. & Ginoux, P. (2022). Enhanced dust emission following large wildfires due to vegetation disturbance. *Nature Geoscience*, 15(11), 878–884. Number: 11 Publisher: Nature Publishing Group.

Zaremba, L. L. & Carroll, J. J. (1999). Summer Wind Flow Regimes over the Sacramento Valley. *Journal of Applied Meteorology and Climatology*, 38(10), 1463–1473. Publisher: American Meteorological Society Section: Journal of Applied Meteorology and Climatology.

https://doi.org/10.5194/egusphere-2023-2827
Preprint. Discussion started: 4 January 2024

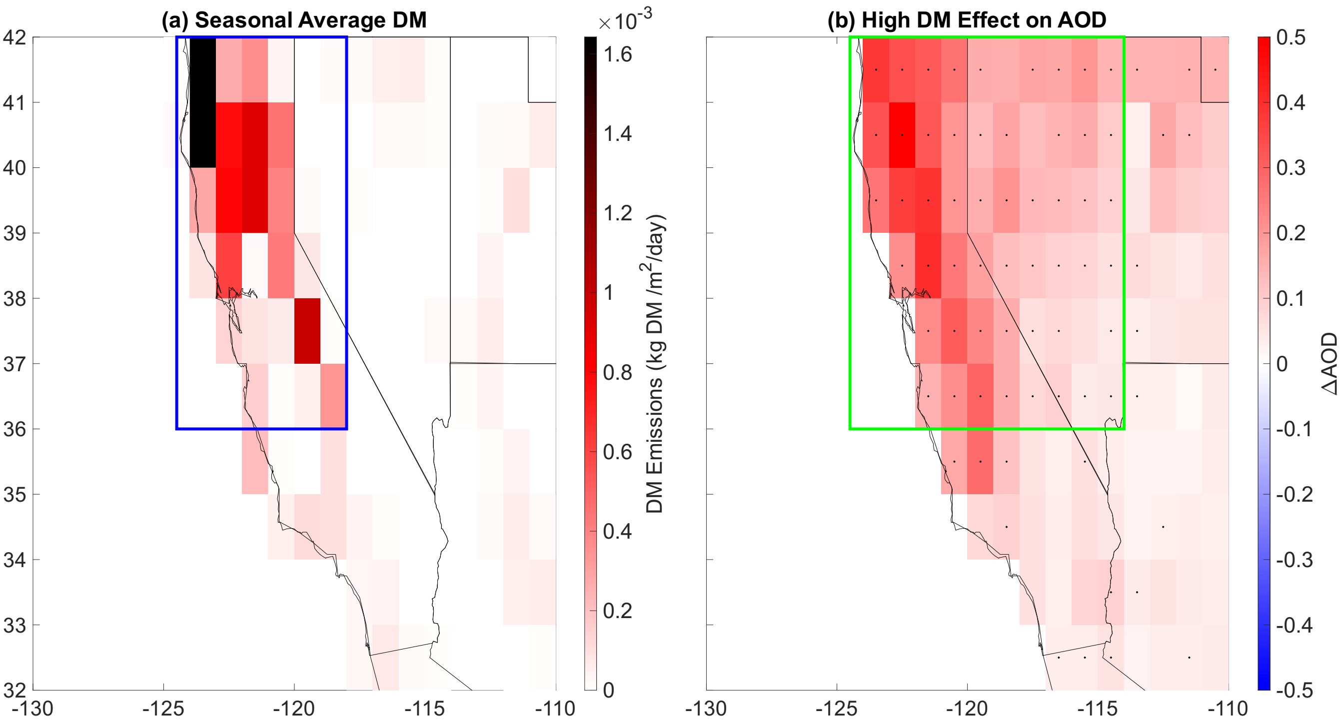

Figure 1. Distribution of fires and the corresponding aerosol optical depth AOD anomaly impacts. (a) average daily fire dry matter DM emissions for the southwestern United States. Blue box signifies the nCA (northern California) region, where average daily fire emissions are the highest. (b) 2003-2022 June-October daily Deep Blue MODIS Aerosol optical depth (AOD) difference between average AOD on 90th percentile DM ($DM90$) and average AOD on 10th percentile DM ($DM10$) days within the 2003-2022 June-October time frame. ΔAOD represents $AOD(DM90) - AOD(DM10)$. Green box symbolizes the nCA-NV (northern California-Nevada) region, where increases in AOD and changes in cloud properties (**Figure 9**) are most significant. Black dots represent statistically significant differences at 90% confidence according to a two-tailed test.

https://doi.org/10.5194/egusphere-2023-2827
Preprint. Discussion started: 4 January 2024

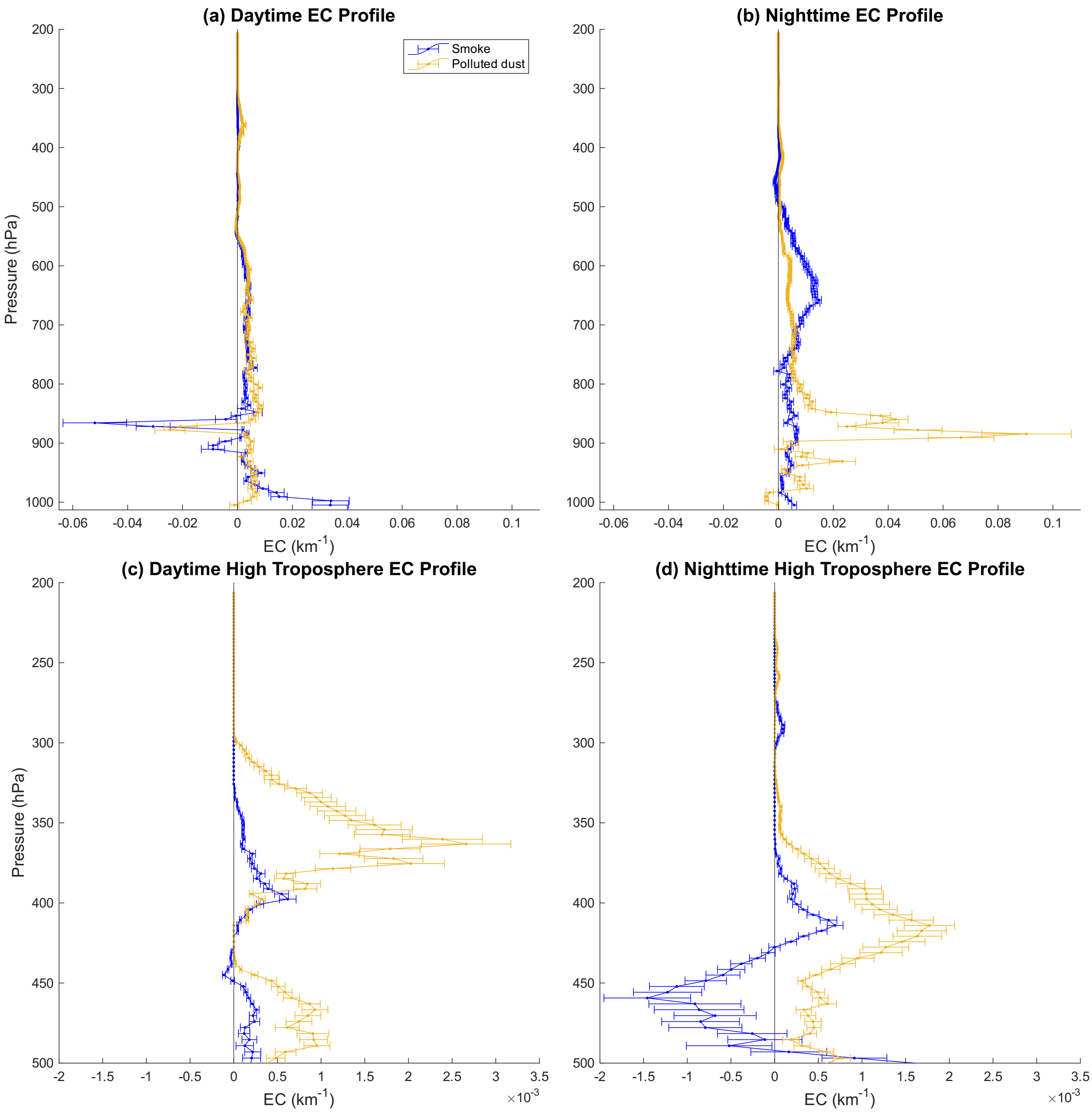

Figure 2. Aerosols extinction coefficient EC profiles on high minus low fire months. Difference in 2006-2021 northern California/Nevada (nCA-NV) regional average CALIPSO EC profiles that occur in 90th percentile northern California (nCA) fire emission months and 10th percentile nCA fire emission months within the 2006-2021 June-October time frame. Blue represents the smoke EC profile, and gold represents the polluted dust EC profile. (a,c) depict the daytime CALIPSO retrievals, while (b,d) depict nighttime CALIPSO retrievals. (a) and (b) display the entire vertical EC profiles, while (c,d) display the profiles in the high troposphere (pressures less than 500hPa). Error bars represent standard errors.

https://doi.org/10.5194/egusphere-2023-2827
Preprint. Discussion started: 4 January 2024

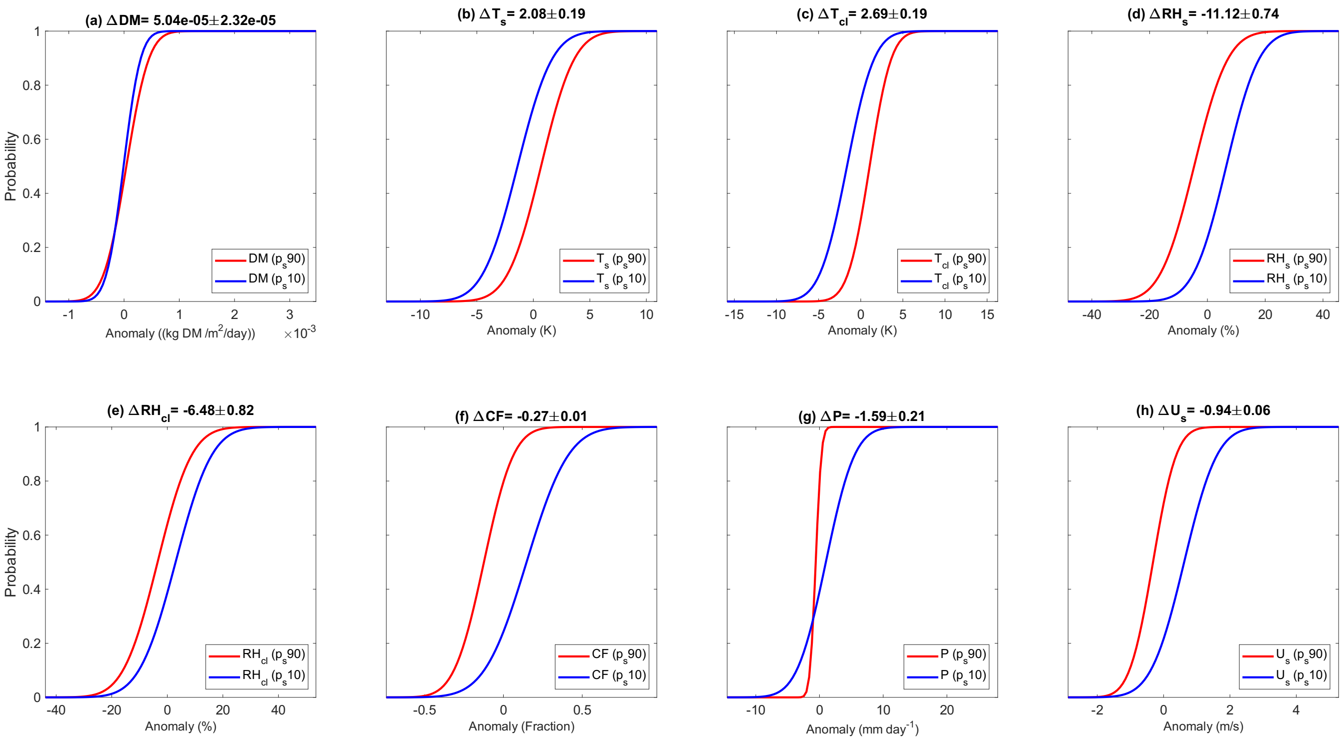

Figure 3. Dependence of meteorological variables on high versus low surface pressure. Regional average cumulative distribution functions (CDFs) for variable anomalies stratified by 90th percentile surface pressure (p_s90) days (red) and 10th percentile (p_s10) (blue) days within the 2003-2022 June-October time frame. Variables depicted include (a) northern California (nCA) fire dry matter (DM) emissions, (b) northern California-Nevada (nCA-NV) surface temperature T_s, (c) nCA-NV cloud layer (700-250hPa) average temperature T_{cl} , (d) nCA-NV surface relative humidity RH_s, (e) nCA-NV cloud layer average relative humidity RH_{cl} , (f) nCA-NV cloud fraction CF, (g) nCA-NV precipitation P, and (h) nCA-NV surface wind speed U. Δ represents the difference between the variable's average anomaly for p_s90 and p_s10 days.

https://doi.org/10.5194/egusphere-2023-2827
Preprint. Discussion started: 4 January 2024

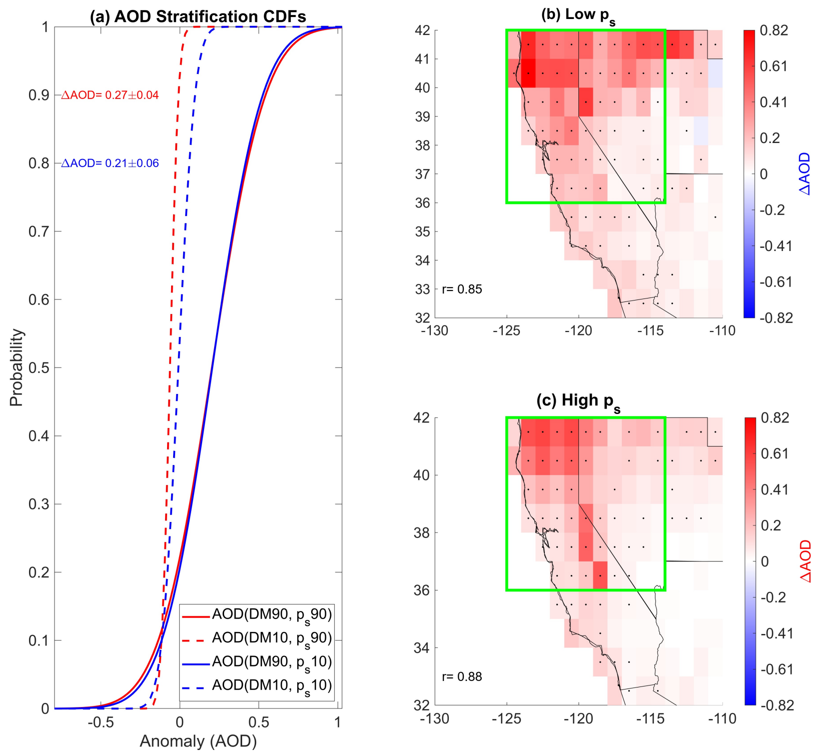

Figure 4. Difference in aerosol optical depth AOD on high and low surface pressure p_s days. Daily northern California-Nevada (nCA-NV) AOD anomalies stratified by p_s and northern California (nCA) fire dry matter DM emission extremes within the 2003-2022 June-October time frame. (a) displays cumulative distribution functions for daily June-October 2003-2022 daily northern California-Nevada (nCA-NV) AOD stratified by high (90th percentile) nCA DM emissions and high nCA-NV p_s $AOD(DM90, p_s90)$ (solid red line),low (10th percentile) DM and high p_s $AOD(DM10, p_s90)$ (dashed red), high DM/low p_s $AOD(DM90, p_s10)$ (solid blue line), and low nCA DM/low p_s $AOD(DM10, p_s10)$ (dashed blue line). The red ΔAOD represents the difference between the solid red and dashed red line $AOD(DM90, p_s90)$-$AOD(DM10, p_s90)$ and the blue ΔAOD represents the difference between the solid and dashed blue lines $AOD(DM90, p_s10)$-$AOD(DM10, p_s10)$. (b) Depicts a map of $AOD(DM90, p_s10)$-$AOD(DM10, p_s10)$ with the nCA-NV region highlighted in the green box. Pearson cross correlation coefficient r between ΔAOD and nCA DM emissions is depicted in the top left corner. (c) Depicts a map of average $AOD(DM90, p_s90)$-$AOD(DM10, p_s90)$. Black dots in (b),(c) represent statistically significant differences at the 90% confidence interval according to a two-tailed test.

https://doi.org/10.5194/egusphere-2023-2827
Preprint. Discussion started: 4 January 2024

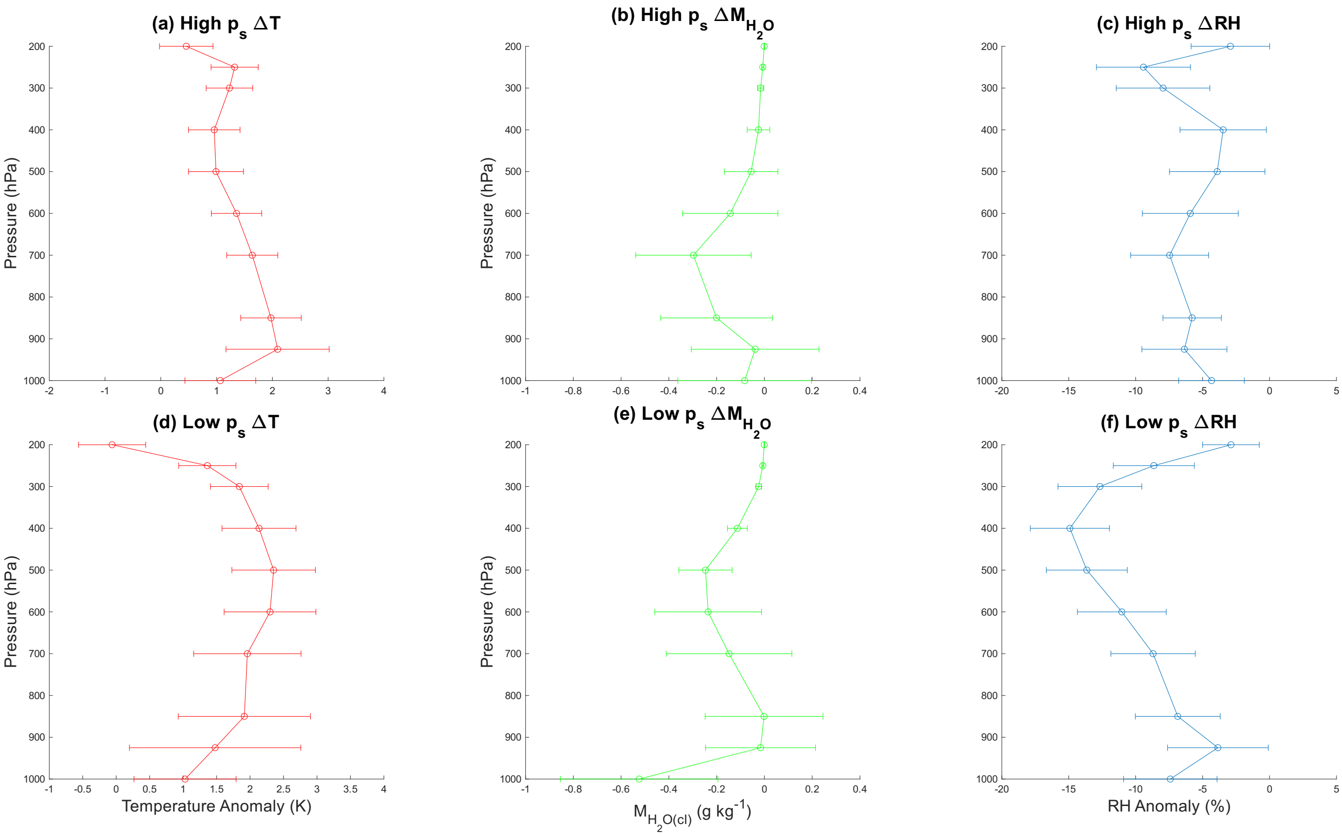

Figure 5. Responses in temperature T, water mass mixing ratio M_{H_2O}, and relative humidity RH profiles to large fires under high and low surface pressure p_s extremes. Northern California-Nevada regional-temporal average differences in T, water mass mixing ratio M_{H_2O} and relative humidity RH profiles between high (90th percentile) and low (10th percentile) northern California fire dry matter emissions DM anomalies stratified by days of high and low p_s anomaly extremes in the 2002-2023 fire season (June-October) time frame. (a,b.c) represent T, M_{H_2O}, and RH differences between high and low fire days on high p_s days. (d,e,f) represent T, M_{H_2O}, and RH differences between high and low fire days on low p_s days. Error bars represent standard error.

https://doi.org/10.5194/egusphere-2023-2827
Preprint. Discussion started: 4 January 2024

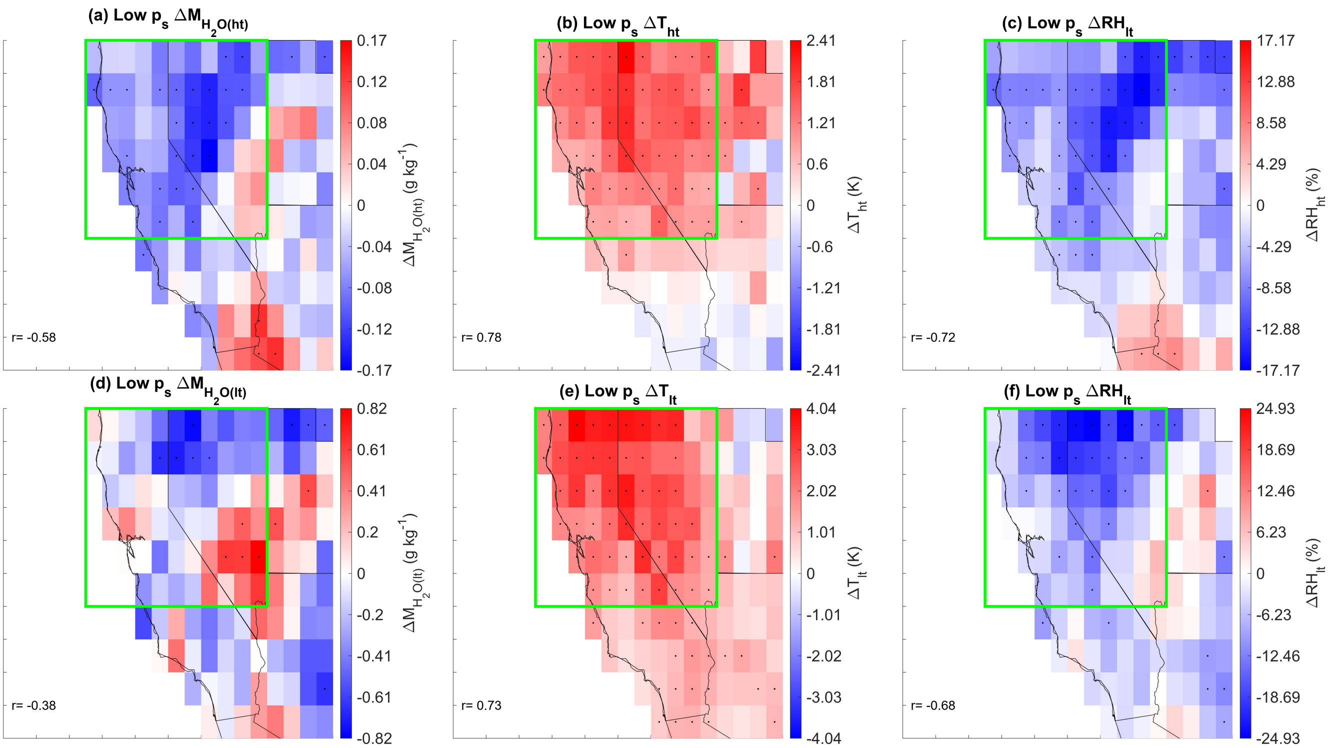

Figure 6. Contributions of specific humidity and temperature to changes in relative humidity in the high and low troposphere. Average high (90th percentile) minus low (10th percentile) fire dry matter emission DM days (in the 2002-2022 June-October timeframe) water mass mixing ratio, temperature, and relative humidity anomalies in the high (500-200hPa) and low/mid (700-500 hPa) troposphere during low surface pressure p_s. Low (10th percentile) pressure extreme 90th minus 10th percentile DM seasonal average anomalies for (a) high troposphere water mass mixing ratio $M_{H_2O(ht)}$, (b) high troposphere temperature T_{ht}, (c) high troposphere relative humidity RH_{ht}, (d) low/mid troposphere water mass mixing ratio $M_{H_2O(lt)}$, (e) low/mid troposphere temperature T_{lt}, and (f) high troposphere relative humidity RH_{lt}. Black dots represent statistically significant differences at the 90% confidence interval according to a two-tailed test. Green box represents northern California-Nevada region. r-value represents Pearson cross correlation coefficient between the given variable and aerosol optical depth at zero lag.

https://doi.org/10.5194/egusphere-2023-2827
Preprint. Discussion started: 4 January 2024

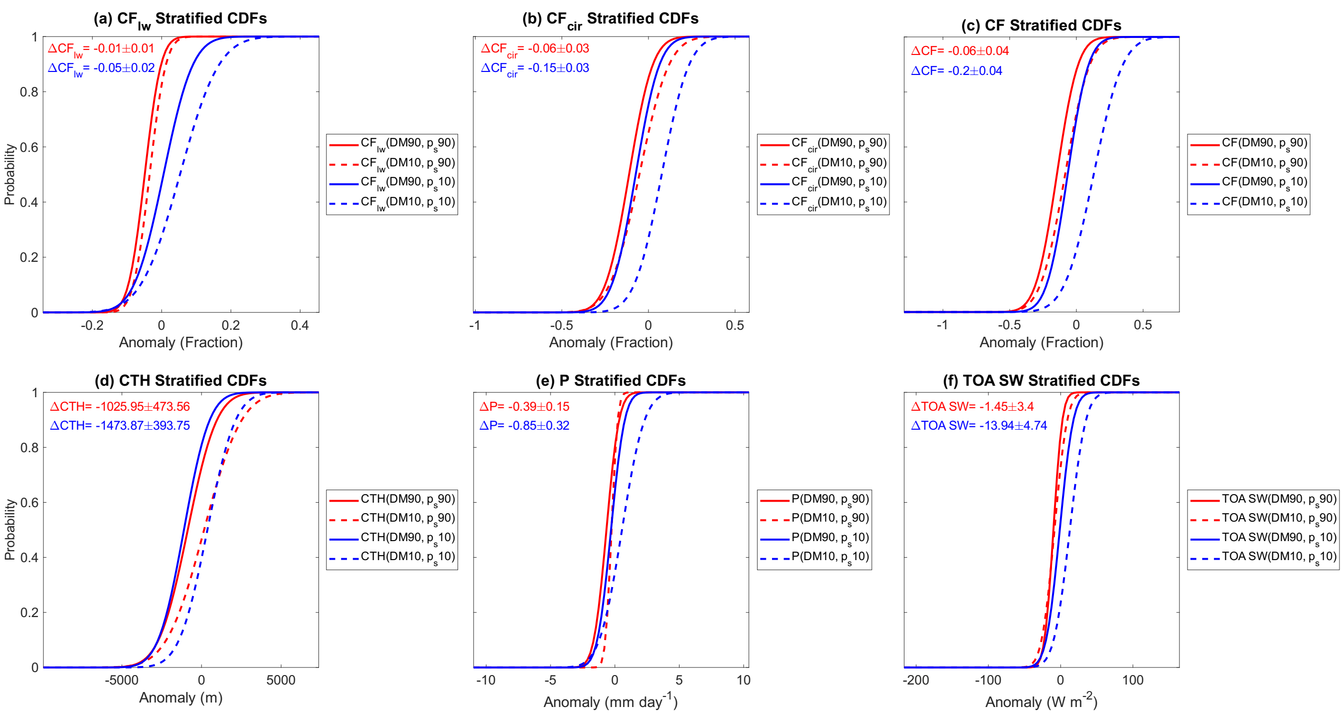

Figure 7. Dependence of meteorological variables to high versus low surface pressure p_s and fires. Cumulative distribution functions (CDFs) for meteorological daily variables' regional average anomalies over the northern California-Nevada (nCA-NV) region in the 2003-2022 June-October timeframe. Solid red line signifies variable anomalies are stratified by high (90th percentile) northern California (nCA) fire dry matter emission DM and high p_s anomaly days ($DM90, p_s90$). The dashed red line signifies variable anomalies are stratified by low (10th percentile) nCA DM and high p_s anomaly days ($DM10, p_s90$). The solid blue line represents variable anomalies are stratified by high nCA DM and 10th percentile p_s anomaly days ($DM90, p_s10$). The dashed blue line symbolizes variable anomalies are stratified by low DM and low p_s anomaly days ($DM10, p_s10$). Variables depicted include (a) cirrus cloud fraction CF_{cir}, (b) liquid water cloud fraction CF_{lw} , (c) cloud fraction CF, (d) cloud top height CTH, (e) precipitation P, and (f) outgoing top of atmosphere shortwave flux $TOA\ SW$. The red Δ represents the differences in the mean of the solid red and dashed red lines ($DM90, p_s90$)-($DM10, p_s90$). The blue Δ represents the differences in the mean of the solid blue and dashed blue lines ($DM90, p_s10$)-($DM10, p_s10$).

https://doi.org/10.5194/egusphere-2023-2827
Preprint. Discussion started: 4 January 2024

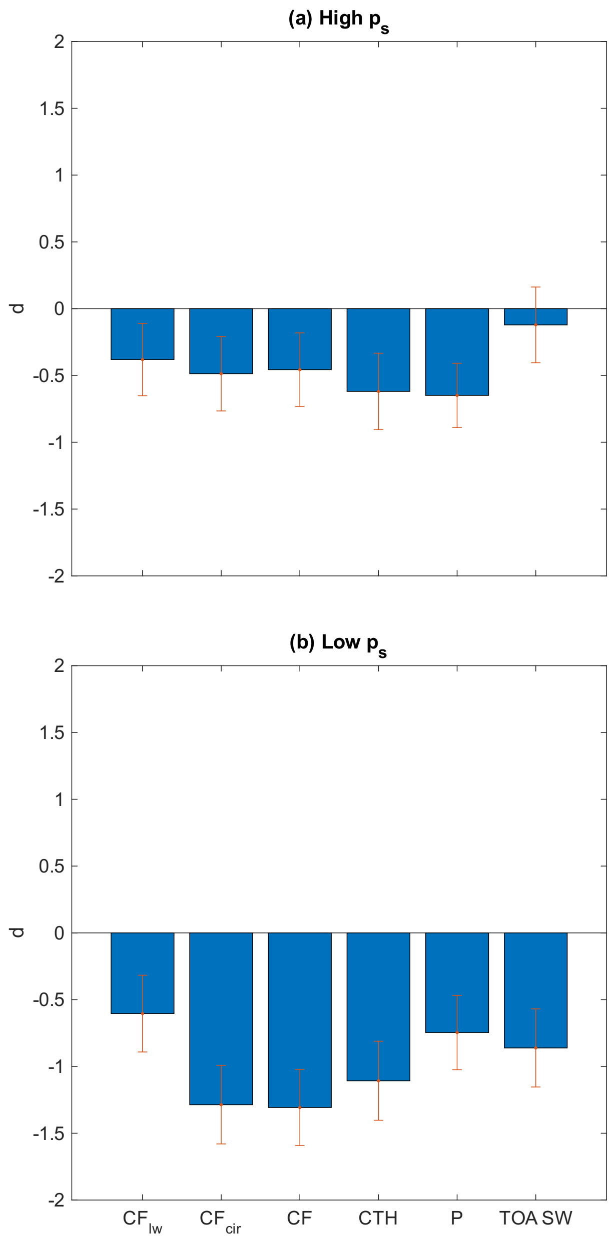

Figure 8. Effect size of large fires on the mean of various meteorological variables. 2003-2022 June-October Cohen's d d values for the difference between northern California-Nevada (nCA-NV) regional averages of variables on high (90th percentile) northern California (nCA) fire dry matter DM emission days and low (10th percentile) nCA DM emission days that coincide with (a) high surface pressure p_s anomaly and (b) low p_s anomaly. Variables include liquid water cloud fraction CF_{lw}, cirrus cloud fraction CF_{cir}, cloud fraction CF, cloud top height CTH, precipitation, and top of atmosphere (TOA) shortwave (SW) flux. (a) represents values of Cohen's d for 90th percentile surface pressure p_s days while (b) represents values of Cohen's d for 10th percentile p_s days. For Cohen's d, values of 0.2 through 0.5 signify a weak effect size, values of 0.5 through 0.8 represent a moderate effect size, and values greater or equal to 0.8 signify a strong effect size. Red bars represent standard error.

https://doi.org/10.5194/egusphere-2023-2827
Preprint. Discussion started: 4 January 2024

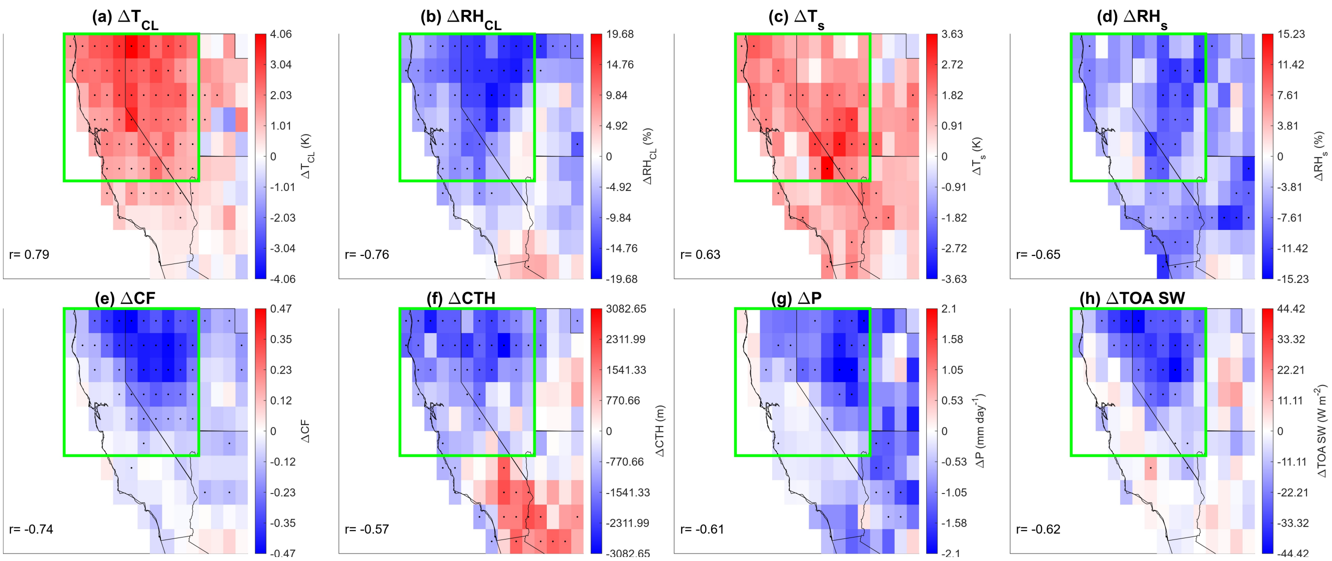

Figure 9. Meteorological responses under high versus low fire days with simultaneously low surface pressure. Difference between average variable anomalies on high (90th percentile) northern California (nCA) fire dry matter DM emission days and low (10th percentile) nCA DM emission days that occur on low surface pressure p_s days in the 2003-2022 June-October time frame. Variables include (a) 700hPa-250hPa average Temperature T_{cl}, 700hPa-250hPa average relative humidity RH_{cl}, (c) surface temperature T_s, (d) surface relative humidity RH_s, (e) cloud fraction CF, (f) cloud top height CTH, (g) precipitation, and (e) top of atmosphere TOA shortwave SW flux. Black dots represent statistically significant differences at the 90% confidence interval according to a two tailed test. Green box symbolizes the northern California-Nevada region. Pearson cross correlation r values in the top left corner of each plot represent the spatial correlation between MODIS Deep Blue aerosol optical depth AOD anomaly and the variable anomaly depicted in the figure. All values of r are significant at the 90% confidence interval according to a two-tailed test.

https://doi.org/10.5194/egusphere-2023-2827
Preprint. Discussion started: 4 January 2024

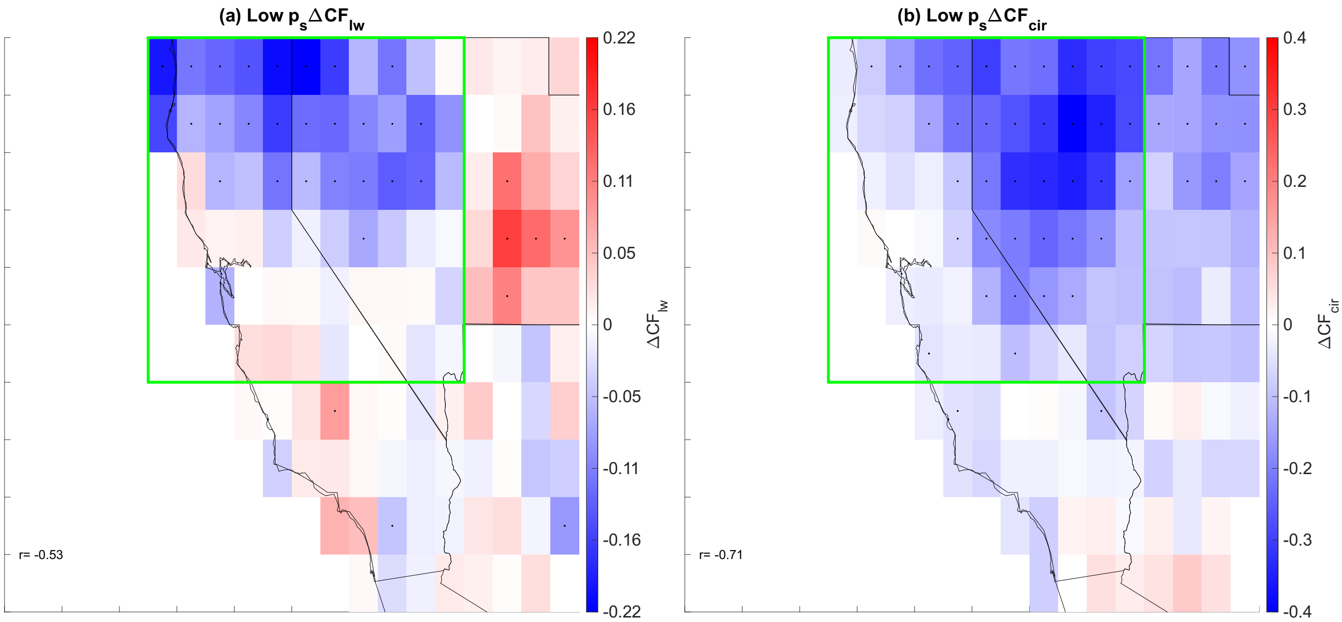

Figure 10. Responses of liquid water and cirrus cloud fraction under high versus low fire days with simultaneously low surface pressure. Difference between average variable anomalies on high (90th percentile) northern California (nCA) fire dry matter DM emission days and low (10th percentile) nCA DM emission days that occur on low surface pressure p_s days in the 2003-2022 June-October timeframe. Variables include (a) liquid water cloud fraction CF_{lw} and (b) cirrus cloud fraction CF_{cir}. Black dots represent statistically significant differences at the 90% confidence interval using a two-tailed test. r represents Pearson cross correlation coefficient values for cross correlations between aerosol optical depth and the variable of interest. The green box represents the northern California-Nevada region. The spatial extent of the changes in CF_{cir} align with the changes in high troposphere water mass mixing ratio in **Figure 6a**, while the changes in CF_{lw} align more with the changes in low/mid troposphere temperature in Figure 6e.

https://doi.org/10.5194/egusphere-2023-2827
Preprint. Discussion started: 4 January 2024

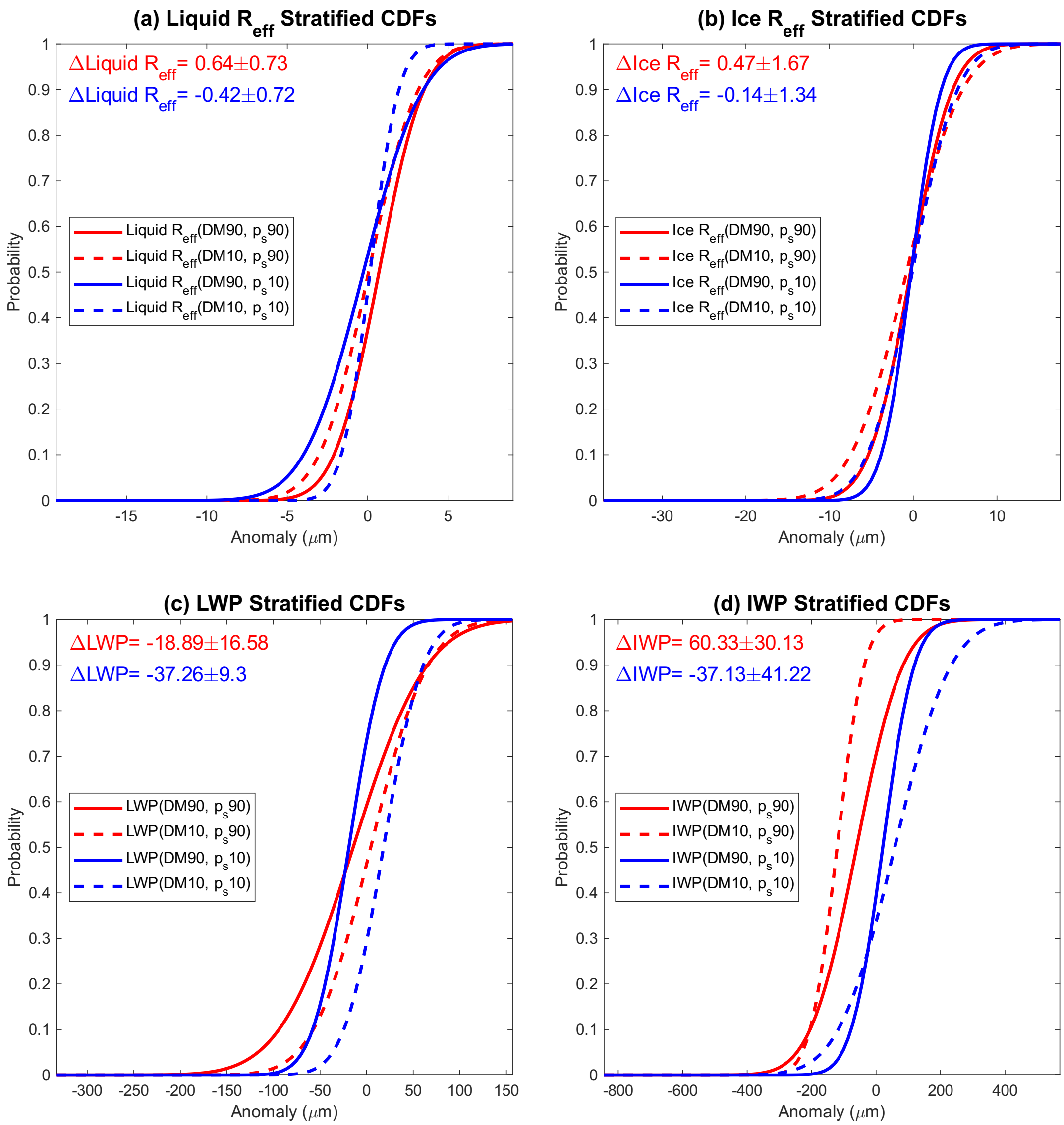

Figure 11. Dependence of microphysical variables to high (90th percentile) versus low (10th percentile) surface pressure p_s and fires. Cumulative distribution functions (CDFs) for cloud microphysical variables' regional average daily anomalies over the northern California-Nevada (nCA-NV) region in the 2003-2022 June-October time frame. Solid red line signifies variable anomalies are stratified by high northern California (nCA) fire dry matter emission DM and high surface pressure p_s anomaly days ($DM90, p_s90$). The dashed red line signifies variable anomalies are stratified by low DM and high p_s anomaly days ($DM10, p_s90$). The solid blue line represents variable anomalies are stratified by high DM and 10th percentile p_s anomaly days ($DM90, p_s10$). The dashed blue line symbolizes variable anomalies are stratified by low nCA DM and p_s anomaly days ($DM10, p_s10$). Variables depicted include (a) liquid effective radius R_{eff}, (b) Ice R_{eff}, (c) liquid water path LWP, (d) and ice water path IWP. The red Δ represents the differences in the mean of the solid red and dashed red lines ($DM90, p_s90$)-($DM10, p_s90$). The blue Δ represents the differences in the mean of the solid blue and dashed blue lines ($DM90, p_s10$)-($DM10, p_s10$).